学位論文

Rhythmic A-to-I RNA editing revealed by comprehensive analysis of CLOCK-controlled genes

(ゲノムワイドな CLOCK の標的探索が明らかにした A-to-I RNA 編集リズム)

平成 26 年 12 月博士(理学)申請

東京大学 大学院理学系研究科 生物化学専攻

寺 嶋 秀 騎

Abstract

In the circadian clock in mammals, which is composed of a transcription-translation feedback loop, CLOCK-BMAL1 complex rhythmically binds to DNA to transactivate a series of the target genes driving the circadian molecular oscillation. Our previous study identified a large number of CLOCK-binding sites in mouse liver by chromatin immunoprecipitation-sequencing (ChIP-Seq) and rhythmically expressed RNAs and miRNAs by RNA-Seq analysis. In the present study, comparative analysis of CLOCK-ChIP-Seq and RNA-Seq of poly (A)+ RNA and small RNA revealed the importance of circadian regulation of post-transcriptional events, such as alternative splicing and miRNA-mediated gene silencing. Among them, I found that *Adar2* (*Adenosine deaminase acting on RNA 2*, also known as *Adarb1*) has CLOCK-binding sites in its first intronic region, and rhythmically expressed in mouse liver. ADAR enzymes bind to double-stranded RNA (dsRNA) and hydrolytically convert adenosines (A) to inosines (I), which is called A-to-I RNA editing. RNA-Seq analysis demonstrated that A-to-I RNA editing levels in the transcripts shows a robust change in a time-of-day-dependent manner, peaking in the late afternoon. Rhythmic A-to-I RNA editing events were attenuated in the Bmal1-deficient or the *Adar2*-deficient mice. Furthermore, Deep-sequencing analysis also revealed that *Adar2* is essential for normal mRNA expression rhythms of a great number of genes, suggesting the significant effect of A-to-I RNA editing on RNA abundance rhythms. Moreover, *Adar2* plays an important role for precise circadian period in both mRNA oscillation and locomotor activity rhythms with abnormal accumulation of CRY2 protein. Collectively, I elucidated the CLOCK-mediated post-transcriptional regulations and the functional crosstalk between A-to-I RNA editing and circadian rhythm.

Table of Contents

1 Introduction

Most organisms have self-sustaining time-keeping mechanisms referred as circadian clocks, which align internal physiological conditions to daily environmental changes with an approximate 24hr period. In mammals, the circadian clocks are located in almost every cell in the body such as liver, and these individual oscillators need to be synchronized within the tissue by the master clocks of hypothalamic suprachiasmatic nucleus (SCN) (Mohawk et al., 2012). The mammalian circadian clocks are composed of auto-regulatory transcription-translation feedback loops (TTFL) (Asher and Schibler, 2011; Dunlap, 1999; Hastings et al., 2003; Reppert and Weaver, 2002). The positive factors in the feedback loops consist of basic helix-loop-helix (bHLH)-PAS transcription factors, CLOCK and BMAL1, which form a heterodimer and bind to canonical CACGTG E-box and noncanonical E-box sequences (CACGTT, CACGNG, and CATG[T/C]G) (Yoshitane et al., 2014) to promote transcription of thousands of clock-controlled genes including *Per* and *Cry*. On the other hand, the negative factors in the feedback loops, PER and CRY, bind to the CLOCK-BMAL1 complex resulting in suppression of the E-box-dependent transactivation including their own transcription. TTFL is an essential mechanism to produce robust 24 h rhythms of various gene expression and circadian outputs such as sleep wake cycle, hormone rhythm and blood pressure (Fig. 1).

Recently, in the circadian clock, posttranslational modifications such as phosphorylation and ubiquitination regulate the function and stability of core clock proteins leading to robust oscillations with the stable period (Gallego and Virshup, 2007; Hirano et al., 2013; Kon et al., 2014; Lee et al., 2001; Yoshitane et al., 2009, 2012). In addition to posttranslational modifications, the importance of post-

transcriptional modifications in circadian mechanisms has become clear over the last decade (Kojima et al., 2011; Lim and Allada, 2013). For example, post-transcriptional regulations such as RNA methylation, IRES-mediated translational regulation, mRNA stability, alternative splicing, polyadenylation, and miRNA-mediated gene silencing were found to play key roles in the modulation of circadian systems (Chen et al., 2013; Du et al., 2014; Fustin et al., 2013; Kim et al., 2010; Kojima et al., 2012; McGlincy et al., 2012; Woo et al., 2009, 2010). Intriguingly, several studies indicated that a large fraction (about 75%) of rhythmically expressed mRNAs exhibit no significant transcriptional rhythm, suggesting a large effect of post-transcriptional regulation on generation of mRNA abundance rhythms (Koike et al., 2012; Menet et al., 2012).

In the present study, I addressed the questions, how CLOCK regulates a large number of transcripts oscillation, and how large post-transcriptional regulation contribute to the circadian outputs. I revealed the complicated mechanisms that CLOCK-mediated various regulations such as indirect transcriptional regulations and rhythmic miRNA-mediated gene silencing. Furthermore, I elucidated the functional interaction between circadian rhythm and A-to-I RNA editing at the molecular and physiological levels for the first time.

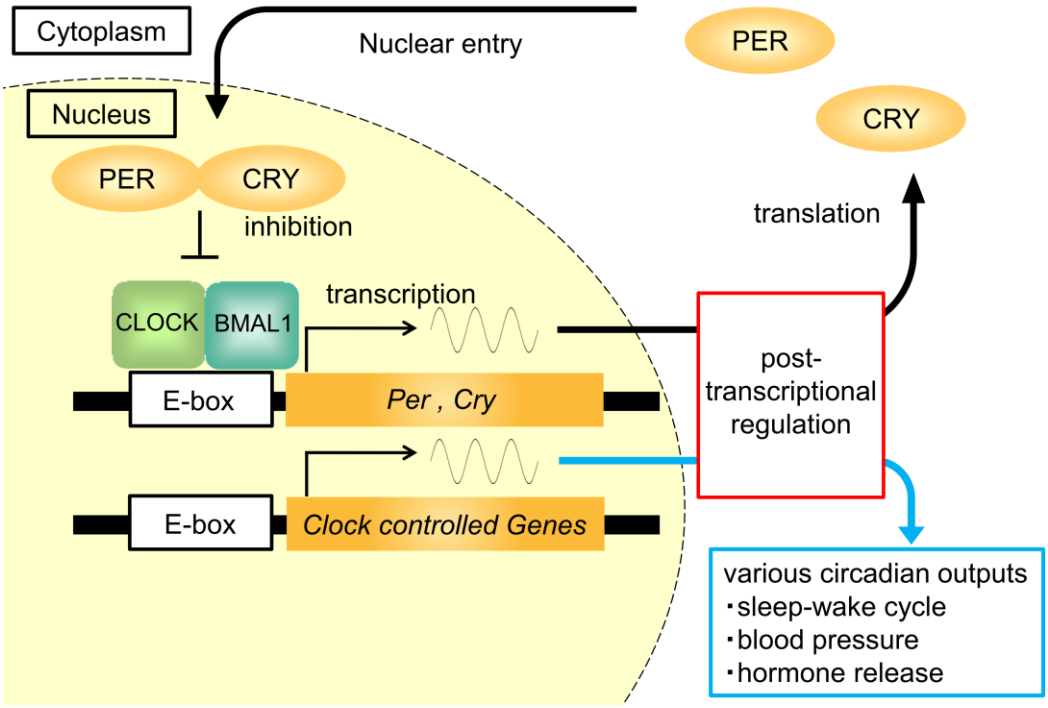

Figure 1　Transcriptional-translational feedback loop in circadian clock

2 CLOCK-ChIP-Seq and RNA-Seq reveal the rhythmic post-transcriptional regulations

2.1 Introduction

In the circadian cycling of gene expression, previous study elucidated that the important mechanism that CLOCK/BMAL1 complex rhythmically binds to genomic regions of E-boxes sequences (Fig. 2) (Ripperger and Schibler, 2006). In addition, circadian phosphorylation of CLOCK and BMAL1 were previously reported (Huang et al., 2012b; Kondratov et al., 2006; Yoshitane et al., 2009), which were thought to be an pivotal regulation for rhythmic activity of the CLOCK-BMAL1 complex binding to the E-boxes. Previously, we performed CLOCK-ChIP-Seq for comprehensive identification of *in vivo* CLOCK-binding sites in mouse liver, and enumerated the functional noncanocical E-box sequences (Yoshitane et al., 2014). Furthermore, our RNA-Seq and small RNA-Seq analyses illustrated various oscillating mRNAs, ncRNAs and miRNAs.

In this study, I focused my attention on CLOCK-mediated indirect regulations such as transcription factors and post-transcriptional regulations. I revealed the presence of novel rhythmic genes, such as Krüppel-Like Factor (KLF) transcription factors, lncRNAs and miRNAs, which were under the regulation of rhythmical CLOCK-binding. In addition, rhythmically regulated alternative-splicing events were also examined by qRT-PCR, which were predicted in RNA-Seq dataset in our laboratory. These indirect regulations should have significant effects on circadian outputs in addition to transcription-translation feedback loops.

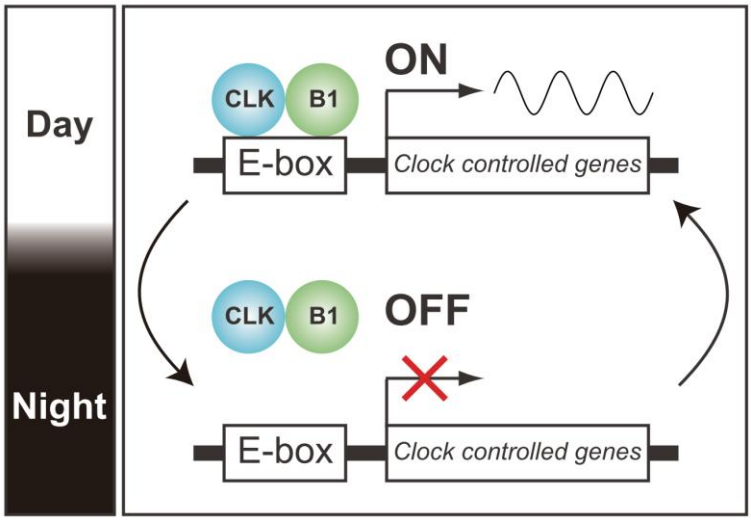

Figure 2 Rhythmic binding of CLOCK/BMAL1 complex to DNA

CLOCK/BMAL1 complex binds to enhancer element called E-box in a circadian manner and transactivates thousands of clock controlled genes (Ripperger and Schibler, 2006).

2.2 Materials and Methods

2.2.1 Animals

The animal experiments were approved by the animal ethics committee of the University of Tokyo. C57BL/6J mice were individually housed in cages with commercial chow (CLEA Japan) and tap water available *ad libitum* under the controlled environment (temperature 22 ± 2°C humidity 65 ± 10%).

2.2.2 RNA preparations

Mice liver were isolated at 6 time points per day three times after thirty-eight hours from the beginning of constant dark conditions (projected CT). The total RNA was prepared from mouse liver by using miRNeasy Mini Kit (QIAGEN) according to the manufacturer's protocol, and was used for qRT-PCR experiments.

2.2.3 Cell culture and dual luciferase assay

HEK293T cells that were maintained in Dulbecco's modified Eagle's medium supplemented with 10% fetal bovine serum. Following plasmids were transiently transfected to HEK293T cells in 12-well plates by using Lipofectamine Plus reagent (Invitrogen) to quantify activities of CLOCK-BMAL1 transactivation. 200 ng BMAL1/pcDNA3.1 and 200 ng Myc-CLOCK/pSG5 in combination with 20 ng firefly luciferase plasmids of pGL3 promoter vectors that harbors various genomic sequences including E-box and E-like box elements as a reporter, and 1 ng renilla luciferase plasmids of pRL-SV40 as an internal control. Reporter plasmids were constructed as previously described (Sasaki et al., 2009). The inserted sequences were as follows: for Klf11 (5'- CCCGG ACCAA AACAC GTGCC GCCGC CCGCC -3'), Klf13 (5'-

TACAG GCACC TGCTG CTCCA TGTGC TTCTG -3'), 0610005C13Rik (5'- CTGAG CCAGG TGTGG TGGCA CACGT GCCTG TC -3'), mir-148a (5'- CCTCC TCAGG GTCAC GTGCG CGCTG GGCGG -3'), mir-150 (5'- CGGGT TGGGA AACAC GTGCT GGGAT TCAGT -3'), mir-802-proximal (5'- GGACG CTGTT CGCAC GTGCC TGGGG TGTCC -3'), mir-802-distal (5'- TTATT TAGCT CTCAC GTGGA ATTTG TTAGA -3'), E4bp4 (5'- GAGAG ACACG TGCTT GACAC ACACG TGGGG CAC -3). The total amount of the transfected plasmids was adjusted at a constant level by the addition of empty vector. The transfected cells were harvested 36 hr after the transfection, and the cell lysates were subjected to dual luciferase assays by luminometry (Promega) according to the manufacturer's protocol.

To test the miR-802-mediated gene silencing of Cav1 through 3'UTR, Cav1-3'UTR luciferase reporter vector was constructed by inserting Cav1-3'UTR fragment into the Xho1 site of pGL3-promoter vector (downstream of the firefly luciferase). For expressing miR-802, the genomic regions at around *pri-miR-802* was amplified from mouse genome and cloned into pcDNA3.1 digested by BamHI and XhoI. Following plasmids were transiently transfected to HEK293T cells in 12-well plates by using Lipofectamine Plus reagent (Invitrogen). 1,000 ng miR-802/pcDNA3.1 and 100 ng Cav1-3'UTR /pGL3 in combination with 20ng renilla luciferase plasmids of pRL-SV40 as an internal control. The cloning primers used for constructions were shown in Table 1.

2.2.4 qRT-PCR

The total RNA prepared at every time points was reverse transcribed by using Go Script reverse transcriptase (Promega) with both an anchored (dT) 15 primer and a random oligonucleotide primer according to the manufacturer's protocols. quantitative RT-

PCR (qRT-PCR) analyses were performed by using StepOnePlus™ Real-Time PCR System (Lifetechnologies) with the gene-specific primers shown in Table1.

2.3 Results

2.3.1 Krüppel-Like Factor (KLF) family as circadian transcription factors

Our CLOCK-ChIP-Seq and RNA-Seq data revealed 324 rhythmic transcripts under the regulation of CLOCK binding (Yoshitane et al., 2014). On the other hand, our dataset also showed that the presence of rhythmic transcripts which exhibited no significant CLOCK-binding, suggesting the importance of indirect regulation for circadian outputs. In fact, gene ontology (GO) analysis identified a lot of rhythmically expressed transcription factors as CLOCK targets. Among them, I remarked Krüppel-Like Factor (KLF) family members were supposed to be CLOCK targets from our deep-sequencing dataset. CLOCK-ChIP-Seq tags were found in the loci of the *Klf11* and *Klf13* gene, including a CACGTG canonical E-box and noncanonical E-boxes near the CLOCK-ChIP peaks, respectively (Fig. 3A). qRT-PCR revealed that *Klf11* and *Klf13* mRNAs were actually expressed in a circadian manner in mouse liver (Fig. 3B). I confirmed that CLOCK/BMAL1 transactivated these genes through the genomic sequences around the CLOCK-binding sites by dual luciferase reporter assays (Fig. 3C). In addition, our laboratory previously showed circadian expression of *KLF10* and the presence of E-box in its promoter region (Hirota et al., 2010), where rhythmic binding of CLOCK was also detected. Furthermore, the other Krüppel-Like Factor (KLF) family members were found to show rhythmic expression and have CLOCK binding sites in their gene loci, for example, *Klf9, Klf15* and *Klf16* genes (Fig. 4). Interestingly, the molecular phylogeny of Krüppel-like family members based on their functional and phylogenetic similarities revealed that *KLF9, 10, 11, 13* and *16* are all categorized to group 3 of KLF family (Fig. 4). They commonly have mSin3a-binding domain and show repressor activity through their interaction with co-repressor mSin3A. The only exception is Klf14, which exhibits no expression and has not yet been

established the physical interaction with mSin3A. Collectively, these data suggested that CLOCK-regulated KLF family members should have important roles in rhythmic expression of their target genes, and contribute to global circadian outputs.

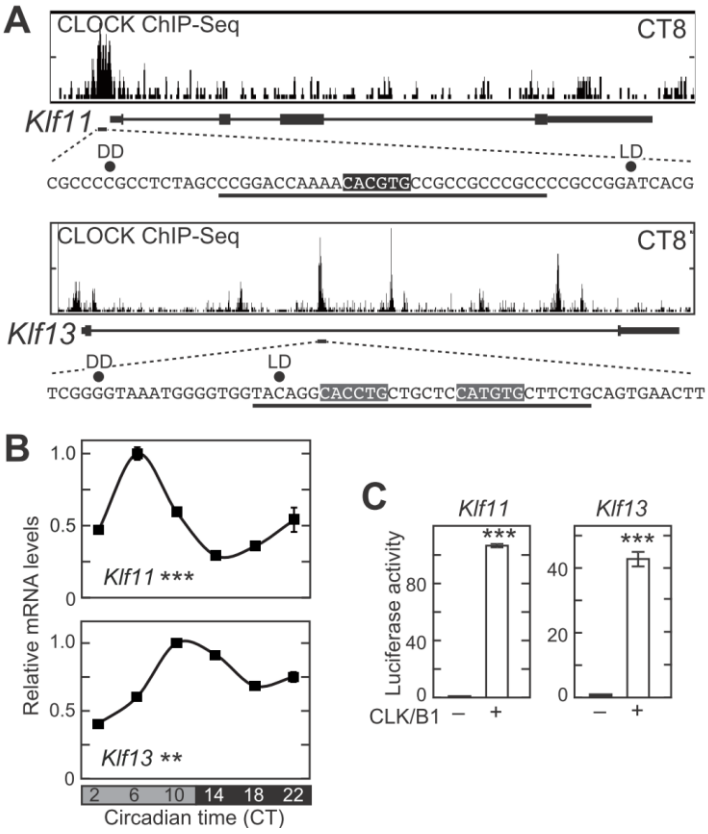

Figure 3 CLOCK/BMAL1-dependent transactivation of *Klf11* and *Klf11*

(A) The genomic sequences and the sequenced tags of CLOCK ChIP-Seq data at around the *Klf11* loci in mouse liver at CT 8 and CT 20, modified from Yoshitane *et al.* (Yoshitane et al., 2014). Closed circles marked with LD and DD indicate the peak positions of CLOCK ChIP-Seq tags at ZT8 and CT8, respectively, modified from Yoshitane *et al.* (Yoshitane et al., 2014). Closed and shaded boxes indicate CACGTG-type E-box and the one-mismatched sequences, respectively. Underlined DNA sequences were used for dual luciferase reporter assay. (B) Circadian expression profiles of *Klf11* quantified by qRT-PCR analysis in mouse liver. The signals were normalized to *Tbp* for each sample and the mean value at the peak time was set to 1 (mean ± SEM; $n = 3$). Change over time was analyzed by one-way ANOVA, ** = $p < 0.01$, *** = $p < 0.001$. (C) CLOCK/BMAL1-dependent transactivation of *Klf11* revealed by dual luciferase reporter assay in HEK293T cells. The mean ratio of firefly to renilla luciferase signals without expression of CLOCK and BMAL1 were set to 1 (mean ± SEM; $n = 3$, *** = $p < 0.001$ by Student's t-test, versus without CLOCK and BMAL1).

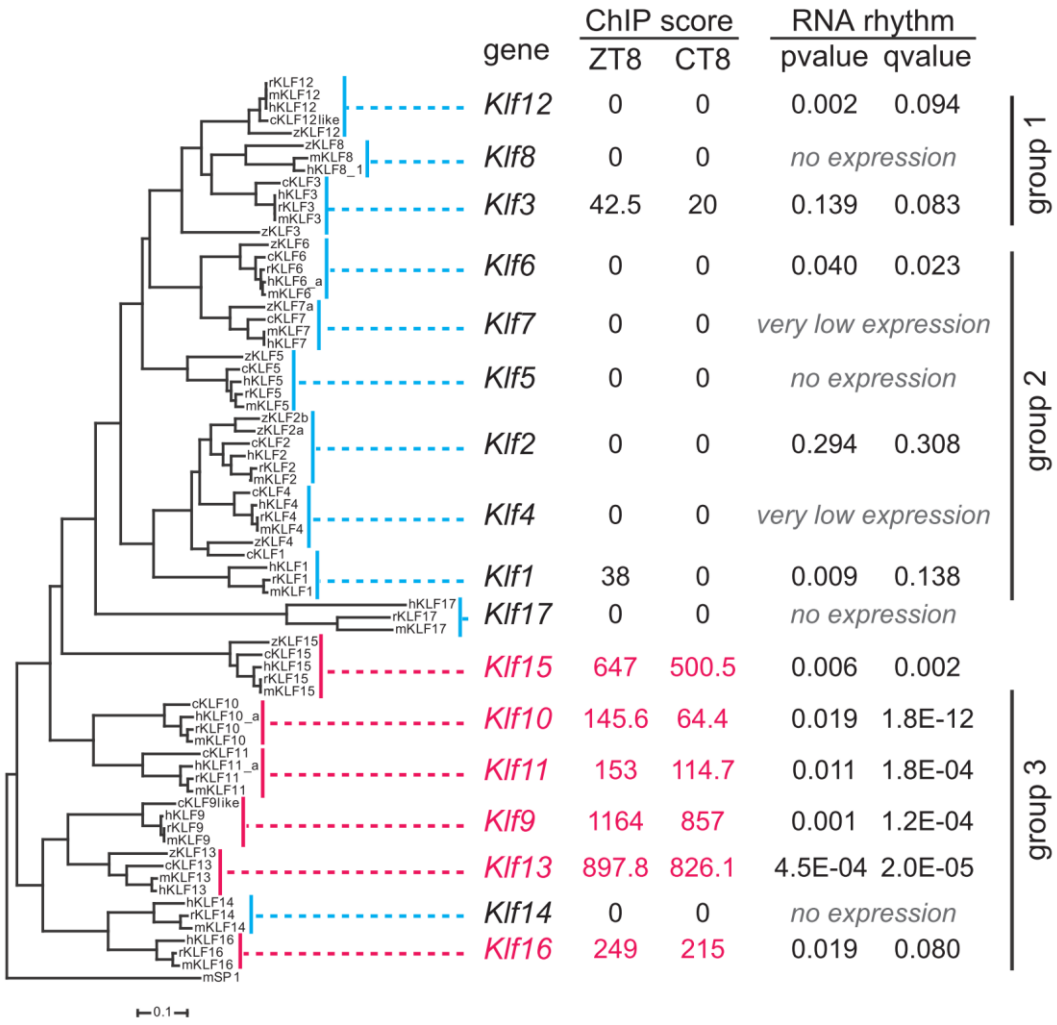

Figure 4 Circadian regulation of KLF transcription factors

Molecular phylogeny of Krüppel-like family members. ClustalX tool version 2.1 was used for creation of sequence alignment and a neighbor-joining tree. The full-length amino acids sequences of the KLF family members were analyzed and mouse SP1 was examined as outgroups (h, human; r, rat; m, mouse; c, chicken; z, zebrafish). Three distinct groups were defined previously (McConnell and Yang, 2010) according to their functional and phylogenetic similarities. CLOCK-ChIP-Seq scores, *p*-values of gene expression rhythmicities, and *q*-values indicating significance of changes in expression of *Klf* transcripts are shown.

2.3.2 Rhythmic posttranscriptional regulation by alternative splicing

Transcribed mRNA precursors (pre-mRNAs) are processed to produce various mRNA isoforms through alternative splicing, which are translated into related proteins with qualitatively distinct functions. Previously, very few studies referring the relationship of circadian rhythm and alternative splicing were reported in mammals (McGlincy et al., 2012; Preußner et al., 2014). Therefore, I focused on the circadian regulation of alternative splicing events.

Circadian variation of the cassette-type alternative splicing were investigated from the RNA-Seq data in Yoshitane *et al.* By counting the numbers of RNA-Seq tags aligned to splice junctions, eighty-three exons were identified as rhythmic cassette-type ones whose spliced patterns changed throughout the day. Among them, I revealed circadian profiles of the alternative splicing of Mink1 (*Misshapen-like Kinase 1*) and Ubqln1 (*Ubiquilin 1*) transcripts by quantitative RT-PCR with splice-junction primers (Fig. 5). Rhythmically spliced mRNAs likely produce circadian differences of protein isoforms and their functions. MINK1 is classified as the germinal center kinase family member, and activates JNK pathway to play an important role in cytoskeleton reorganization, cell adhesion and cell motility (Hu et al., 2004). JNK pathway were found to be important for mammalian circadian clockwork (Yoshitane et al., 2012), so that the differently spliced isoforms of Mink1 might cause distinct regulation on circadian rhythms. Moreover, UBQLN1 is an important component of ubiquitination machinery to proteasome, and directly associates with *Presenilin1* or *2*, which are known to generate β-amyloid (Haapasalo et al., 2011). A significant association between a risk for Alzheimer's disease and an increased expression level of alternatively spliced isoform lacking exon 8 of the UBQLN1 transcript were reported (Bertram et al., 2005). Circadian expression profiles of alternatively spliced isoform

of *Ubqln1* including exon 8 (Fig. 5) suggest the possible mechanism that disordered circadian rhythms lead to the increased risk for Alzheimer's disease. What splicing factors cause circadian alternative splicing events remain to be elucidated. Note that a splicing factor of PTBP1 (*Polypyrimidine tract binding protein*) were rhythmically expressed and the CLOCK binding were observed in the *Ptbp1* gene locus. PTBP1 binds to pyrimidine-rich sequences like as UCUU, which are observed near the alternative exons of Mink1 and Ubqln1, suggesting the time-of-day dependent regulation of RNA splicing pattern and their function was one of the important post-transcriptional regualtion by circadian clock.

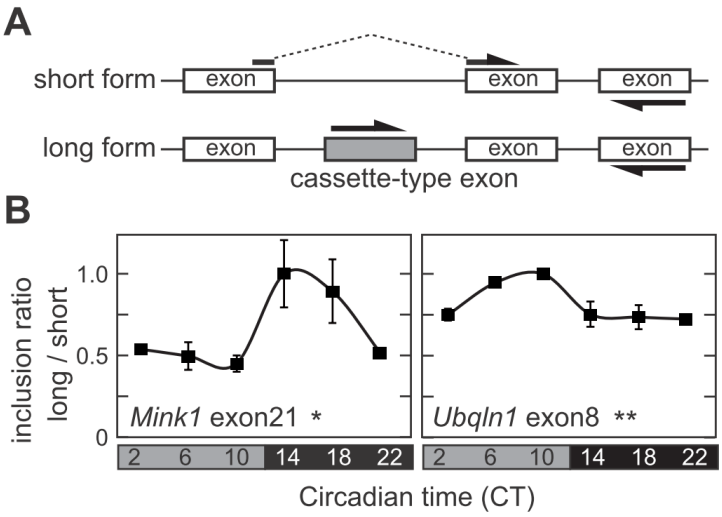

Figure 5 Circadian regulation of alternative splicing

(A) A scheme of primers for qRT-PCR analysis. (B) Time-of-day dependent alternative splicing events revealed by qRT-PCR.

2.3.3 Circadian regulation of long non-coding RNAs

Recently, long non-coding RNAs (lncRNAs) have come to be of special interest with advances in sequencing technologies revealing a large number of lncRNAs. lncRNAs are thought to be involved in regulating gene expression through epigenetic processes (Plath et al., 2002). Our CLOCK-ChIP-Seq and RNA-Seq showed that some lncRNAs had CLOCK-binding sites in their gene loci, and rhythmically expressed in mouse liver. I investigated the CLOCK-ChIP-Seq data in Yoshitane *et al.* and examined the gene expression profiles of 0610005C13Rik lncRNAs. The CLOCK binding was detected at its third intron harboring at least one functional E-box (Fig. 6A). Consistently, 0610005C13Rik mRNAs showed rhythmic expression by qRT-PCR in mouse liver (Fig. 6B). Dual luciferase assay showed the CLOCK/BMAL1-dependent transactivation through the intronic E-boxes (Fig. 6C). The presence of CLOCK-controlled lncRNAs were confirmed by these data, suggesting important mechanisms that lncRNAs contribute to circadian outputs of gene expression rhythms.

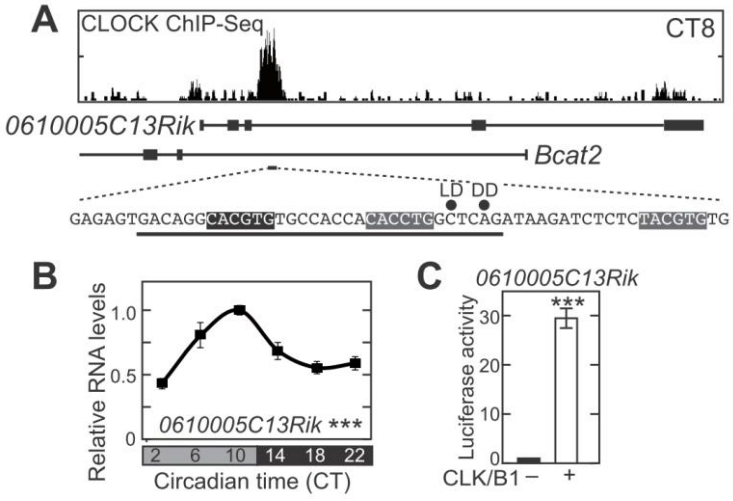

Figure 6 CLOCK/BMAL1-dependent transactivation of ncRNA

Circadian regulation of *0610005C13Rik* regulated by CLOCK/BMAL1 was revealed. Statistics and abbreviations as in Fig. 3.

2.3.4 Rhythmically controlled post-transcriptional regulation mediated by miRNAs

Previous study reported that some miRNAs exhibit robust circadian rhythms of expression, and they show significant effects on the circadian oscillation itself and various circadian outputs such as metabolic pathway (Cheng et al., 2007; Gatfield et al., 2009; Vollmers et al., 2012). I comprehensively searched rhythmically expressed miRNAs in our small RNA-seq dataset, and found *mir-148a-3p*, *mir-150-3p* and *mir-802-5p* were expressed in a circadian manner in mouse liver. qRT-PCR analysis confirmed rhythmic expression profiles of *mir-150-3p* (Fig. 7A). Dual luciferase reporter assay confirmed that CLOCK/BMAL1 transactivated these genomic sequences near the CLOCK-binding sites in their loci (Fig. 7B). To confirm the rhythmic transcription of precursor miRNAs, qRT-PCR was performed by using primers at the stem-loop for quantification of primary miRNAs. *pri-mir-802* was rhythmically expressed, suggesting that the CLOCK/BMAL1-dependent transcription caused miRNA expression rhythms (Fig. 8A). Rhythmically expressed miRNAs likely produce circadian profiles of transcripts targeted by miRNA-mediated gene silencing. TargetScan, which is a program of computational prediction for miRNA targets, predicted *Cav1* (*Caveolin-1*) is a putative target of miR-802, and indeed, the previous study confirmed that prediction (Lin et al., 2011). I also demonstrated that a luciferase reporter harboring *Cav1* 3'UTR transiently transfected in HEK293T cells exhibited decreased activity by the overexpression of miR-802 (Fig. 8B). Note that no distinct circadian profiles of Pol II occupation was found in the *Cav1* gene locus indicating that its transcript were not transcribed in a circadian manner (Le Martelot et al., 2012). However, *Cav1* mRNA showed circadian expression profiles, and steady-state levels of *Cav1* transcripts were suppressed when the *pri-mir-802* expression reached a peak phase (Fig.8A). These data demonstrated a possible mechanism that the circadian

profiles of mRNA abundance were regulated by rhythmically expressed miRNAs.

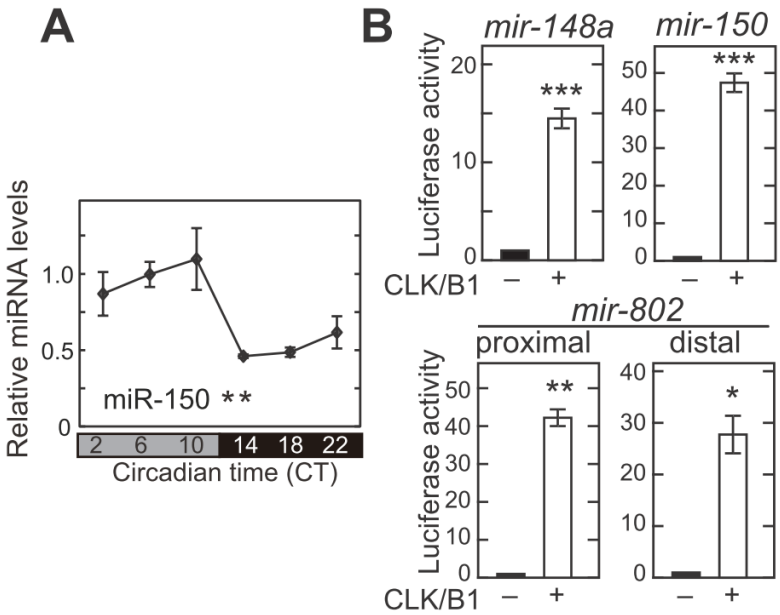

Figure 7 Rhythmically expressed miRNAs transactivated by CLOCK/BMAL1
(A) qRT-PCR analysis revealed rhythmically expressed miR-150. (B) CLOCK/BMAL1-dependent transactivation of miRNAs revealed by dual luciferase reporter assay in HEK293T cells. Statistics and abbreviations as in Fig. 3.

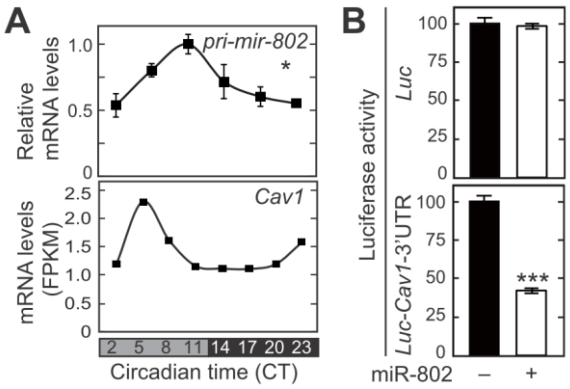

Figure 8　Rhythmic gene silencing of *Cav1* transcripts regulated by miR-802

(A) Circadian expression profiles of *pri-mir-802* quantified by qRT-PCR analysis. The signals were normalized to *Tbp* for each sample and the mean value at the peak time was set to 1 (mean ± SEM; $n = 3$). Change over time was analyzed by one-way ANOVA, * = $p < 0.05$. (B) The gene silencing effect of mir-802 on Cav1 3'UTR in HEK293T cells were analyzed by dual luciferase reporter assay. Statistics and abbreviations as in Fig. 3.

2.4 Discussion

The improvement in sequencing technology enabled us to perform variety of sequencing analyses and describe the genome-wide cellular state under different conditions, including time-of-day differences. Several transcriptome analyses of circadian rhythms were recently performed (Koike et al., 2012; Menet et al., 2012; Vollmers et al., 2012), however, they did not mention the significant role of indirect regulations in circadian outputs. In the present study, I revealed the indirect regulations through CLOCK-controlled KLF transcription factors, and found various post-transcriptional regulations.

Recent study elucidated that KLF15 contributes to circadian expression of KChIP2 gene in order to regulate the duration and pattern of myocardial repolarization resulting in circadian QT interval variation in the heart (Jeyaraj et al., 2012a). In addition, *Klf15* was also identified as clock-dependent peripheral regulator for nitrogen homeostasis rhythms in liver through controlling the expression of enzymes involved in nitrogen homeostasis (Jeyaraj et al., 2012b). Furthermore, *Klf9* was found to be a rhythmic transcription factor modulating keratinocyte proliferation in a circadian manner (Spörl et al., 2012). Intriguingly, the molecular phylogeny of Krüppel-like family members revealed the suggestive enrichment of group 3 KLF family members in CLOCK-controlled rhythmic Klf genes. Klf members belonging to group 3 coordinately regulate target genes expression with co-repressor mSin3A, and protein complexes containing mSin3A act as histone deacetylase-dependent corepressors. These facts imply evolutionarily conserved transcriptional regulations by histone modification that regulate circadian outputs by using Klf members. In fact, Weitz laboratory elucidated that PSF (*Polypyrimidine tract binding protein associated splicing factor*) within the

PER complex purified from mouse tissues recruits mSin3A, and subsequently PER complex rhythmically delivers histone deacetylases to the Per1 promoter, resulting in repression of Per1 transcription (Duong et al., 2011). Taken together, a coevolutionary mechanism of mSin3A-dependent circadian transcriptional regulation would be possible.

I validated the presence of some rhythmically expressed miRNAs, and they have CLOCK-binding sites in their gene loci. I realized that the peak phase of rhythmic miRNAs were enriched during the subjective day (data not shown), suggesting the significant effect of CLOCK-controlled transactivation in miRNA accumulation rhythms. Interestingly, our RNA-Seq data showed the circadian profiles of transcripts related to miRNA biogenesis, such as Ago4, suggesting that circadian regulations of miRNA biogenesis could exist in addition to a CLOCK-dependent regulation. Further study is needed.

In the present study, I revealed the pivotal roles of CLOCK-controlled indirect regulations such as rhythmically expressed transcription factors, rhythmic lncRNAs, rhythmic miRNA-mediated gene silencing and circadian changes of alternative splicing events (Fig. 9). CLOCK-controlled KLF family members might regulate rhythmic expression of their target genes, and rhythmic post-transcriptional regulations might be important for adequate circadian physiological outputs.

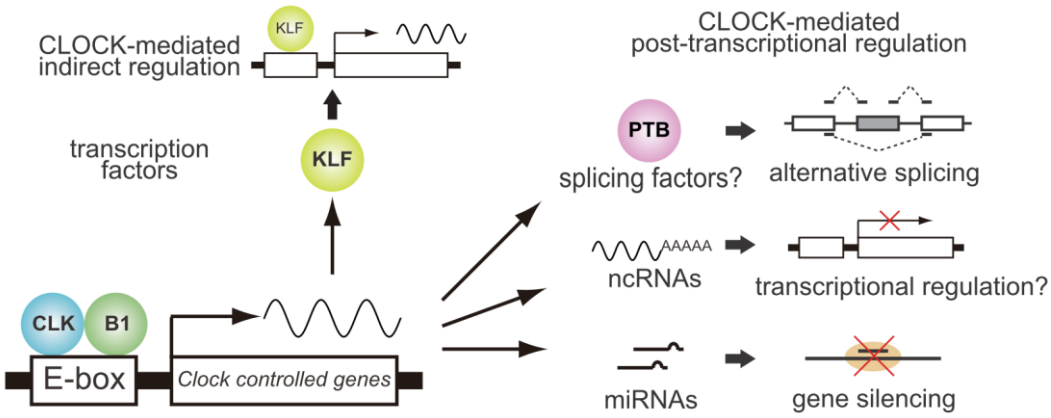

Figure 9 Models for the CLOCK-controlled indirect regulations

3 Adar2 regulates rhythmical A-to-I RNA editing and circadian gene expression

3.1 Introduction

Recent studies showed significant effects of post-transcriptional regulation on generating mRNA abundance rhythms in the mammalian circadian clock. Previous works primarily focused on quantitative post-transcriptional modifications which lead to protein abundance rhythm, such as poly(A) tail length (Kojima et al., 2012), mRNA translation (Jouffe et al., 2013; Lee et al., 2014) and miRNA-mediated gene silencing (Chen et al., 2013; Cheng et al., 2007; Du et al., 2014; Gatfield et al., 2009). Recently, it was shown that the qualitative post-transcriptional modification, that is, RNA-methylation-dependent RNA processing elicits circadian period elongation (Fustin et al., 2013). However, a role of RNA modification in circadian rhythms is still elusive.

In our previous chromatin immunoprecipitation-sequencing (ChIP-Seq) and RNA-Seq study, we extensively identified 1,629 CLOCK-target genes in the mouse liver (Yoshitane et al., 2014). In order to investigate novel CLOCK-regulated post-transcriptional regulation, I comprehensively searched CLOCK-regulated rhythmic genes from 1,629 CLOCK-target genes in combination with the other three transcriptome data in mouse liver. Here, we found CLOCK rhythmically binds to the intronic regions of *Adenosine deaminase acting on RNA 2* (*Adar2*) gene locus, leading to the rhythmical expression of *Adar2* in mouse liver. A-to-I RNA editing is a post-transcriptional modification catalyzed by the adenosine deaminase acting on RNA (ADAR) enzymes which bind to double-stranded RNA (dsRNA) and hydrolytically convert adenosines (A)

to inosines (I) (Hogg et al., 2011; Nishikura, 2010). As the translation machinery recognizes inosine as guanosine, editing in protein coding regions causes a codon change and leads to subsequent alteration of amino acids sequences. In addition, editing in non-coding RNA molecules such as precursors of microRNAs (miRNAs) regulates the biogenesis of miRNA, and editing in intornic region causes alternative splicing event and nonsense-mediated RNA decay (Mallela and Nishikura, 2012) (Fig. 10). In mammals, three ADAR family members of ADAR1 (*Adar*), Adar2 (*Adarb1*) and Adar3 (*Adarb2*) were identified and alternative promoters give rise to two protein isoforms of ADAR1 (ADAR1 p110, ADAR1 p150), although ADAR3 has not been shown to have any catalytic activity (Chen et al., 2000). A-to-I RNA editing is an essential process, as *Adar1*$^{-/-}$ and *Adar2*$^{-/-}$ mice exhibit embryonic and postnatal lethal phenotypes, respectively (Hartner et al., 2004; Higuchi et al., 2000). One of the important editing sites among *Adar2*-mediated editing is the recoding site of the genomically encoded glutamine (Q) to an arginine (R) residue (known as Q/R site) in the transcript encoding subunit B of the *glutamate-gated ion channel receptors 2* (Gria2), which regulates the calcium permeability of receptors. Genetic engineering of mice to substitute a glutamine for arginine codon for the Q/R site (Gria2$^{R/R}$ mice) averts the early postnatal death in absence of functional *Adar2* gene, demonstrating that the Q/R site within Gria2 is the essential editing for survival (Higuchi et al., 2000). *Adar2*$^{-/-}$ / *Gria2*$^{R/R}$ mice display normal phenotype and life span, however, the physiological role of all ADAR2 substrates have remained to be elucidated.

In the present study, I showed CLOCK-dependent transactivation of *Adar2* leading to rhythmic gene expression. A-to-I RNA editing showed cycling editing levels which were largely abolished not only in *Bmal1*-knockout mice but also in *Adar2*-knockout mice. RNA-Seq analysis in the knockout mouse revealed that *Adar2* is essential for normal

circadian output as the rhythmic mRNA expression of a great number of genes. Intriguingly, the *Adar2*-knockout mice exhibited short period rhythms of gene expression and locomotor activity, with inhibition of translational repression of *Cry2* by let-7 miRNA. Collectively, we elucidated that the qualitative post-transcriptional regulation of A-to-I RNA editing has critical roles of both the circadian oscillation and dynamic circadian outputs, that is, editing rhythms and mRNA abundance rhythms.

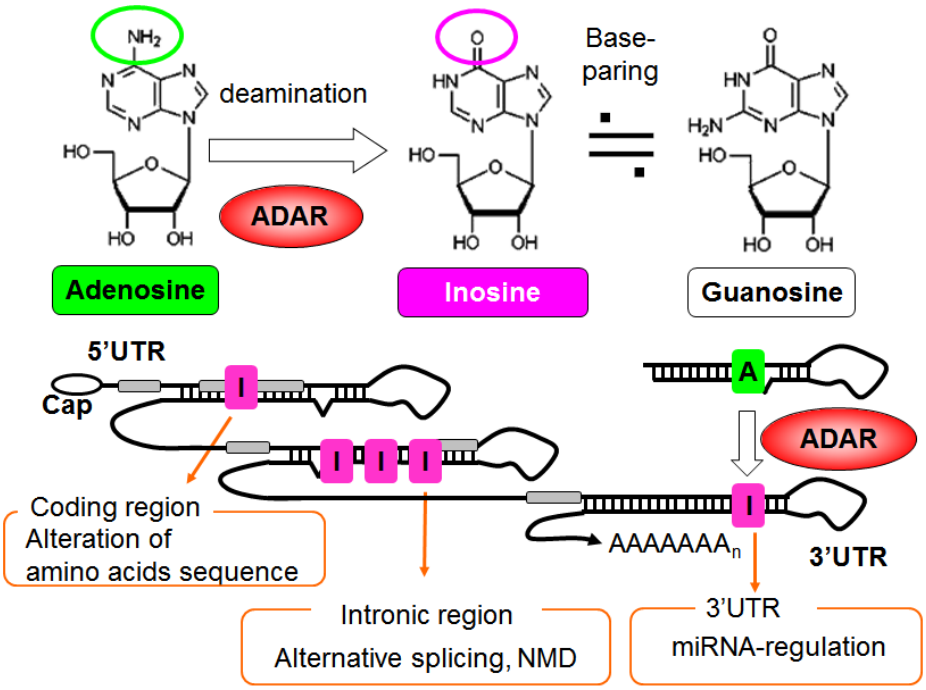

Figure 10 Physiological roles of A-to-I RNA editing

3.2 Materials and Methods

3.2.1 Animals

The animal experiments were approved by the animal ethics committee of the University of Tokyo. C57BL/6J mice, *Bmal1*-knockout mice (C57BL/6J background) (Shimba et al., 2011) and *Adar2*$^{-/-}$ / *Gria2*$^{R/R}$ mice (C57BL/6J background, obtained from Mutant Mouse Regional Resource Centers (MMRRC)) (Higuchi et al., 2000) were individually housed in cages with commercial chow (CLEA Japan) and tap water available *ad libitum* under the controlled environment (temperature 22 ± 2°C humidity 65 ± 10%).

3.2.2 Behavioral experiments

Six- to ten-week-old mice were housed individually in cages equipped with running wheels and were entrained to 12 hr light / 12 hr dark (LD) cycles for at least 2 weeks and released into constant dark (DD) conditions for 21 days or longer. The spontaneous locomotor activities were recorded by wheel revolutions in 5 min bins and analyzed by using ClockLab software (Actimetrics). The circadian period of the activity rhythms under DD conditions were determined by chi-square periodogram procedure, based on locomotor activity in two weeks interval taken 10 days after the start of DD conditions. In the jet lag experiments, the animals were entrained to LD cycles for at least 2 weeks, and then LD cycles were 8-hr phase-advanced and subsequently 8-hr phase-delayed. The amounts of phase advance or phase delay after subjection to the phase-shifted LD cycles were determined by the days required for entrainment.

3.2.3 Cell culture and transfection

NIH3T3 and HEK293T cells were cultured as previously described (Yoshitane et al., 2009). NIH3T3 and HEK293T17 cells were transiently transfected by using

Lipofectamine Plus reagent (Invitrogen) and Lipofectamine 3000 reagent (Invitrogen), respectively, according to the manufacturer's protocols. Plasmids used for transfection are described in each experiment methods.

3.2.4 Plasmids

Mammalian expression vectors encoding FLAG-tagged mouse ADAR2 proteins and shRNAs (short hairpin RNAs) for Adar2 were constructed as described previously (Kurabayashi et al., 2010). For FLAG-ADAR2, an oligonucleotide encoding the FLAG epitope sequence was fused to the 5' end of full-length mouse Adar2 cDNA and cloned into pSG5. The empty pSG5 vector was used for the control of transfection. shRNAs (short hairpin RNAs) were designed by using siDirect (http://sidirect2.rnai.jp/), a Web-based online software program, and the inserted sequences were as follows: 5'- GTGTA TCAAC GGTGA ATACA TGA -3' for shAdar2_1, 5'- GTGGT AGATG GCCAG TTCTT TGA -3' for shAdar2_2, 5'- AAGGT GATAA GTGTT TCGAC AGG -3' for shAdar2_3. A control short hairpin RNA was designed as previously described (Kon et al., 2014). Oligonucleotides to express the shRNAs were inserted into the pSilencer3.1-H1 puro vector (Ambion).

3.2.5 Quantitative RT-PCR (qRT-PCR)

For quantifying gene expression, RNA was reverse transcribed by Go Script Reverse Transcriptase (Promega) with both an anchored (dT)15 primer and a random oligo primer. The cDNA was subjected to real-time PCR (StepOnePlus™Real-Time PCR Systems : Applied Biosystems) by using GoTaq Master Mix (Promega) with the following gene specific primers shown in Table 1. The gene specific primers for Rps29 were previously described (Svingen et al., 2009).

3.2.6 Dual luciferase reporter assay

To quantify CLOCK/BMAL1-dependent transactivation, dual luciferase reporter assay was performed as described previously (Yoshitane et al., 2014). Briefly, HEK293T cells in 12-well plates were transiently transfected with 200 ng Myc-CLOCK/pSG5 and 200 ng BMAL1/pcDNA3.1 in combination with 20 ng of a firefly luciferase plasmid that harbors the intronic regions of *Adar2* gene locus as a reporter, and 2 ng of renilla luciferase plasmid (pRL-SV40) as an internal control. Reporter plasmids were constructed as described (Sasaki et al., 2009). The inserted sequences were as follows: 5'- ACCAT TGCTG AAACC CCGTG AAAAA GATTG GCTTG -3' for E-box1, 5'- ACCAT TGCTG AAACG GCCCT AAAAA GATTG GCTTG -3' for E-box1 mut, 5'- CCTGT CAGTG TTCTC ACGTG GCCAT CCCCA GAAAT -3' for E-box2, 5'- CCTGT CAGTG TTCTG GACCT GCCAT CCCCA GAAAT -3' for E-box2 mut. The total amount of DNA was adjusted by adding the empty expression plasmids.

To quantify the effect of *Adar2* on *Cry2* 3' UTRs reporter expression, NIH3T3 cells in 12-well plates were transiently transfected with 5 ng Luc-Cry2 3'UTR/pGL4.13 in combination with 500 ng of *Adar2* shRNAs and 2 ng of renilla luciferase plasmid (pRL-SV40) as an internal control. For construction of reporter plasmid, the 3'UTR region of the mouse *Cry2* gene (nucleotides from 1 to 1100 or 1101 to 2177) was inserted into the XbaI site of pGL4.13 (Promega). For mutation in the *Cry2* 3' UTR region, the predicted let-7g target sites (nucleotides from 1369 to 1375) sequences were mutated into GCCATAG.

3.2.7 Real-time monitoring of circadian rhythms of cultured cells

Real-time monitoring of luciferase expression was performed by using NIH3T3 cells

expressing a luciferase reporter containing the 0.3-kb promoter region of the mouse Bmal1 gene in combination with 500 ng of Adar2 shRNAs as previously described (Kon et al., 2008).

3.2.8 Direct Sequencing and editing frequency

For quantifying editing frequency, total RNA was reverse transcribed by Go Script Reverse Transcriptase (Promega) with both an anchored (dT) 15 primer and a random oligo primer. The cDNA was amplified by KOD-Plus-Neo (TOYOBO) with the gene specific primers, and then, a second PCR reaction was performed with 80-fold-diluted first RT-PCR product as a template and primers for the second PCR. Gene specific primers were shown in Table1. Subsequently, the amplified cDNA fragments from RT-PCR were treated with ExoSAP-IT (USB) and were directly sequenced on an Genetic Analyzer 3500 (Applied Biosystem) by using the BigDye v3.1 Ready Reaction mix (Applied Biosystems). Editing sites appeared as mixed peaks in traces. Four-dye-trace sequences in abi file format were processed using BioEdit (http://www.mbio.ncsu.edu/BioEdit/bioedit.html). Editing frequency was quantified by measuring maximal height of A peaks (unedited) and G peaks (edited) and calculating percentage of the population edited at each site (100 % × [G height / (A height + G height)]).

3.2.9 Antibodies and immunoblot analysis

Preparation of mouse liver nuclear proteins were described previously (Yoshitane et al., 2009). Liver nuclear proteins were immunoblotted with following antibodies; anti-β-actin, anti-Flag, anti-TBP, anti-PER2 (Alpha Diagnostic International), CLSP3 anti-CLOCK (Yoshitane et al., 2009), B1BH2 anti-BMAL1 (Yoshitane et al., 2009), anti-

CRY1 (Hirano et al., 2013), anit-CRY2 (Hirano et al., 2013), anti-ADAR2 (Bioworld technology).

3.2.10 Preparation of RNA

Mice liver was isolated at 6 time points per day after thirty-eight hours from the beginning of DD conditions (projected CT). For RNA-Seq experiments, total RNA was prepared from mouse liver by using TRIzol reagent (Invitrogen) according to the manufacturer's protocol, and subsequently, poly(A)+ RNA were isolated from the total RNA as the manufacturer's protocol. For quantitative RT-PCR and direct sequencing, total RNA was prepared from mouse liver and NIH3T3 cells by using miRNeasy Mini Kit (QIAGEN) according to the manufacturer's protocol.

3.2.11 Deep-Sequencing

For *Adar2*$^{-/-}$ / *Gria2*$^{R/R}$ mice and the *Adar2*$^{+/+}$ / *Gria2*$^{R/R}$ littermates, purified RNA samples were sequenced on Illumina HiSeq 2500 sequencer (101 bp, paired end), according to the manufacturer's protocol.

3.2.12 Data Availability

Illumina sequencing data for the RNA-Seq (6 time points, with two biological replicates for each time points) are available in the DDBJ/EBI/NCBI databases under the accession numbers DRPXXXXX

3.2.13 Reference sequence and annotation data

The mouse genome sequence was obtained from Ensembl (mm10, http://www.ensembl.org/). The annotated gene models (GRCm38) and the annotations of rRNAs were taken from Ensembl (release 75, http://www.ensembl.org/). The

annotations of tRNAs were retrieved from GTRNADB (http://gtrnadb.ucsc.edu/) (Chan and Lowe, 2009).

3.2.14 Identification of rhythmic editing sites

Sequenced reads were trimmed by cutadapt (Martin, 2011) version 1.5 with the parameters " -q 5 --overlap=15 --minimum-length 50 -a" allowing up to six mismatches. Trimmed reads were mapped to the mouse genome (mm10) by MapSplice (Wang et al., 2010) (version 2.1.8) with paramters "--min-map-len 50 --max-hits 1". bamtools (Barnett et al., 2011) (version 2.3.0) were used for selecting uniquely and properly mapped pairs. 'rmdup' command in samtools (version 0.1.19) were used for removing potential PCR duplicates: if multiple pairs have identical external coordinates, only retain the pair with highest mapping quality. Among the registered editing sites in the database of DARNED and RADAR (Kiran et al., 2012; Ramaswami and Li, 2014), editing sites were detected by in-house programs written in Java. Editing sites having more than 5-read coverage at every time point were considered to be expressed. Editing frequency was calculated if at least three SNV counts were present at editing sites and forward strand ratio was $\geqq$ 0.1 to $\leqq$0.9 in order to avoid strand-specific error. Forward strand ratio means the ratio of reads with SNV on forward strand to those on both strands. Editing frequencies from the two independent six-time points were concatenated and were considered to be rhythmic if the computational program of Circwave (Oster et al., 2006) detects rhythmicity with threshold of $p<0.1$. Heatmaps were generated by the “gplots” package of R by using the function “heatmap2”.

3.2.15 Identification of rhythmically expressed transcripts

For the estimation of gene expression levels, TopHat2 version 2.0.11 (Kim et al., 2013)

was used for mapping sequenced reads to the mouse genome (mm10) (Table 2). bamtools (Barnett et al., 2011) (version 2.3.0) were used for selecting uniquely and properly mapped pairs. 'rmdup' command in samtools (version 0.1.19) were used for removing potential PCR duplicates. Cufflinks version 2.2.1 (Trapnell et al., 2010) was used for estimating the expression level of each gene as fragments per kilobase of exon per million fragments (FPKM) and for detecting differentially expressed genes between *Adar2*$^{-/-}$ / *Gria2*$^{R/R}$ mice and the *Adar2*$^{+/+}$ / *Gria2*$^{R/R}$ littermates at each time point (*q*-value < 0.2). A gene was considered to be expressed if the sum of its FPKM values across the six time points was more than three. FPKM values from the two independent six-time points rhythms were concatenated and a gene was defined as rhythmic if all of three programs, ARSER (Yang and Su, 2010), JTK cycle (Hughes et al., 2010) and Circwave (Oster et al., 2006) detected rhythmicity with threshold of *p*-value < 0.05 and amplitude (maximal/minimal FPKM) >= 1.5. When we considered arrhythmic genes, a more stringent cut-off was used to increase sensitivity, *p*-value >= 0.05 in all of three programs.

3.3 Results

3.3.1 *Adar2* is a direct target of CLOCK-BMAL1 complex

Previously, we reported a genome-wide map of CLOCK binding sites and circadian gene expression by CLOCK-ChIP-Seq and RNA-Seq analyses (Yoshitane et al., 2014). Among 1,126 genes that were rhythmic in our RNA-Seq dataset, 157 genes are enumerated as rhythmic transcript in mouse liver in all of the other three published papers (Koike et al., 2012; Menet et al., 2012; Vollmers et al., 2012) (Fig. 11, Table 3). 81 CLOCK target genes defined by our CLOCK-ChIP-Seq were identified as faithfully rhythmic, including well-known clock genes such as *Per1*, *Per2*, *Per3*, *Dbp*, *Hlf*, *Tef*, *Nr1d1* and *Nr1d2*. Among them, the *Adar2* (*Adarb1*) transcript definitely showed a rhythmical expression profile and CLOCK protein rhythmically binds to two intronic regions in the *Adar2* gene locus (Fig. 12A, B). To determine *Adar2* expression rhythms, total RNAs were prepared from wild-type mouse liver isolated at the 6 time points under constant dark (DD) conditions with three biological replicates at each time points, and were subjected to qRT-PCR. *Adar2* mRNA levels showed significant oscillation with a peak at CT14 (CT represents circadian time under DD conditions, the beginning of DD conditions was defined as CT12) (Fig. 12C, Left Top). The *Adar2* mRNA was constantly kept low throughout the day in *Bmal1*-knockout mice liver (Shimba et al., 2011), where rhythmic expression of known clock-controlled genes was abolished (Fig. 12C, Left Bottom). Three ADAR family members, ADAR1 (*Adar*), ADAR2 (*Adarb1*) and ADAR3 (*Adarb2*), are present in mammals. Alternative promoters in *Adar1* gene give rise to two protein isoforms, ADAR1 p150 and ADAR1 p110, and ADAR3 has not been shown to have any catalytic activity (Chen et al., 2000). The expression levels of the two *Adar1* isoforms *p150* and *p110* showed faint rhythms and mostly constant,

respectively (Fig. 12C, Middle, Right), while Adar3 was not expressed in mouse liver (Menet et al., 2012; Yoshitane et al., 2014). In the promoter assays, CLOCK and BMAL1 activated the transcription through the two *Adar2* intronic sequences, in which CCCGTG noncanonical E-box (in the E-box1 region) and the canonical CACGTG E-box (in the E-box2 region) were found (Fig. 12D). The transcriptional activation was significantly attenuated by introducing a mutation in the E-box (Fig. 12D). ADAR2 protein levels were also found to be rhythmic in wild-type and also in *Adar2*$^{+/+}$ / *Gria2*$^{R/R}$ mice liver (Fig. 13). These data indicate that ADAR2 is rhythmically regulated by CLOCK transactivation, and A-to-I RNA editing is under the circadian control.

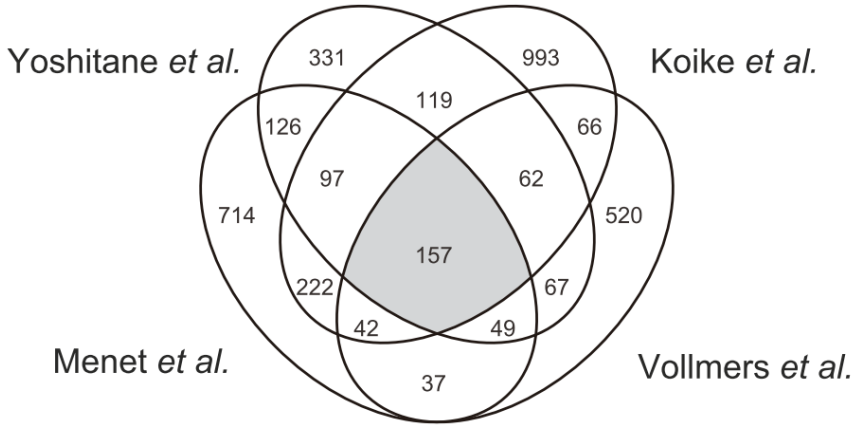

Figure 11 Overlap of rhythmic genes in the four published papers

Overlap of rhythmic genes identified in mouse liver transcripts by RNA-Seq analysis. Yoshitane *et al*. (7), Koike *et al.* (21) and Vollmers *et al.* (23) were examined under DD conditions, and Menet *et al*. (22) were performed under LD conditions.

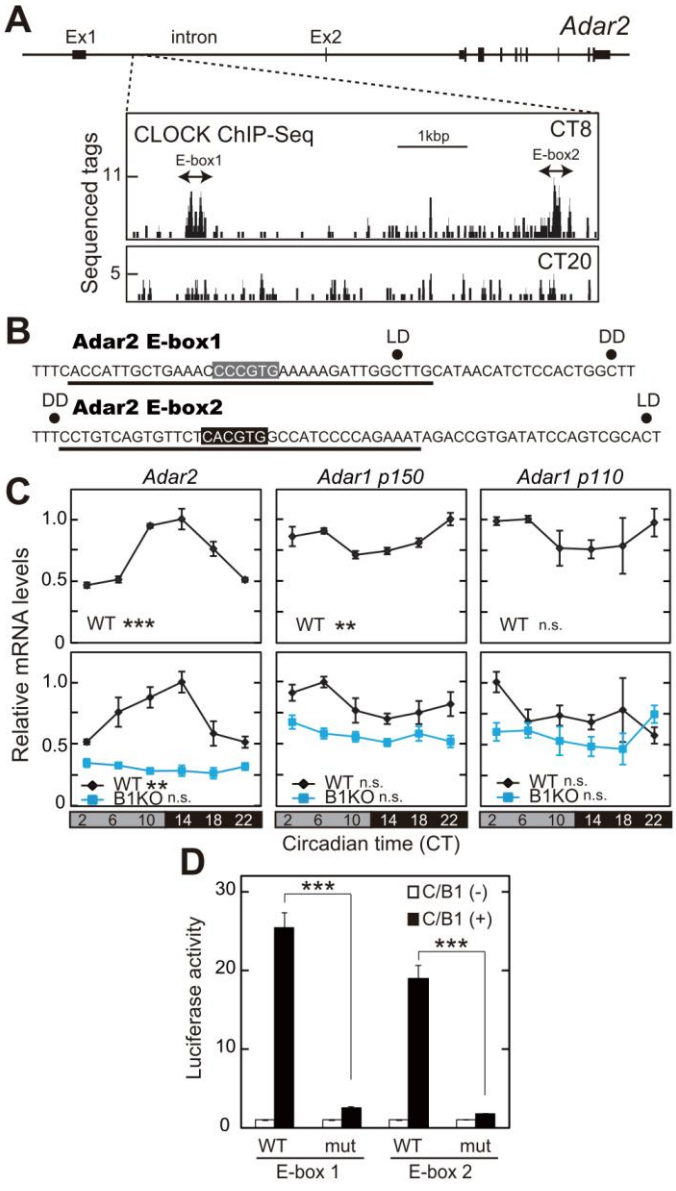

Figure 12 CLOCK/BMAL1-dependent transactivation of *Adar2* in mouse liver

(A) CLOCK ChIP-Seq data at around the *Adar2* loci in mouse liver at CT 8 and CT 20. Two CLOCK-binding sites were named as E-box1 and E-box2, modified from Yoshitane *et al.* (Yoshitane et al., 2014). (B) The genomic sequences in E-box1 and E-

box 2 regions. Closed circles marked with LD and DD indicate the peak positions of CLOCK ChIP-Seq tags at ZT8 (zeitgeber time) and CT8, respectively, modified from Yoshitane *et al.* (Yoshitane et al., 2014). Closed and shaded boxes indicate CACGTG-type E-box and the one-mismatched sequences, respectively. Underlined DNA sequences were examined for transactivation activity in dual luciferase reporter assay in HEK293T cells. (C) Circadian expression profiles of *Adar2, Adar1p150 and Adar1p110* transcript quantified by qRT-PCR analysis in wild-type (Top), *Bmal1*-knockout mice and wild-type littermates (Bottom) mouse liver. The signals were normalized to Rps29 for each sample and the mean value at the peak time was set to 1. Data are means with SEM from three independent mice ($n = 3$). Change over time was analyzed by one-way ANOVA, * = $p < 0.05$, ** = $p < 0.01$, *** = $p < 0.001$, n.s. = $p \geqq 0.05$. (D) E-box1-luc/pGL3, E-box1 mut-luc/pGL3, E-box2-luc/pGL3 and E-box2 mut-luc/pGL3 were used as firefly luciferase plasmids. The values of the luciferase activities were shown as the ratios of bioluminescence signals from firefly luciferase to those from renilla luciferase (internal control). Means of the signal ratios without expression of CLOCK and BMAL1 were set to 1. Data are means with SEM from three independent experiments ($n = 3$, *** = $p < 0.001$ by Student's t-test, versus without CLOCK and BMAL1).

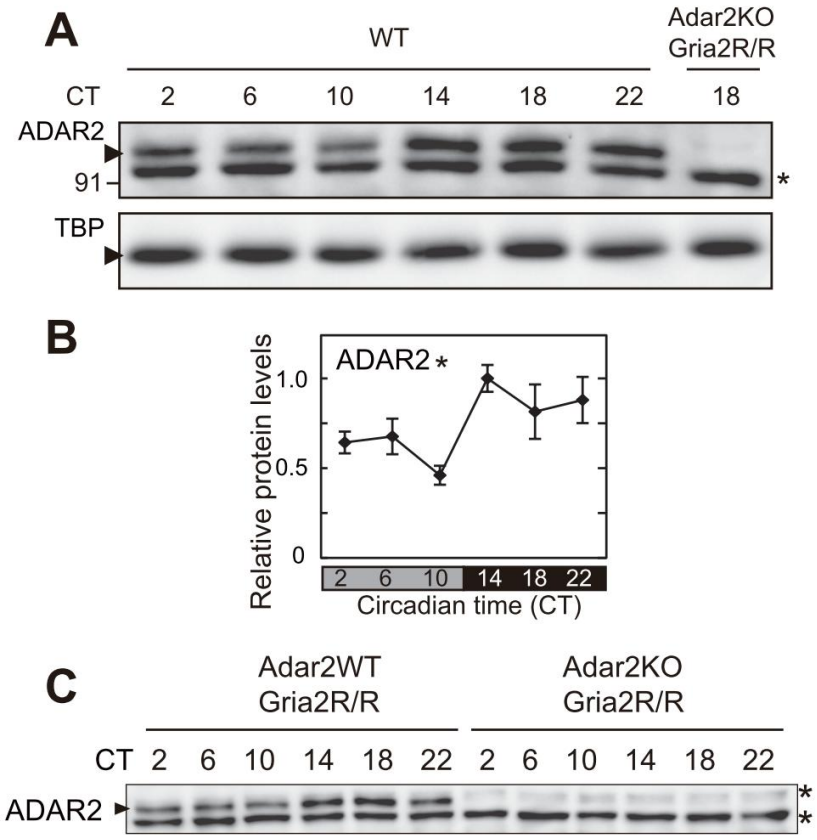

Figure 13 Circadian expression profiles of ADAR2 proteins

(A) Rhythmically expressed ADAR2 proteins in mouse liver indicated by an arrow (top panel). A nonspecific band is indicated by an asterisk. TBP served as a loading control (bottom panel). (B) The band intensities of ADAR2 in (E) are plotted. The signals were averaged from three independent mice and the mean value at the peak time was set to 1. Data are means with SEM (n = 3). Change over time was analyzed by one-way ANOVA, * = $p < 0.05$. (C) Rhythmically expressed ADAR2 proteins in the Adar2-knockout and the littermate wild-type mice liver are indicated by an arrow. A nonspecific band is indicated by an asterisk.

3.3.2 Rhythmic A-to-I RNA editing events regulated by Adar2

The previous studies indicated that the editing level [G / (A+G) (%)] could be reliably assessed by the relative heights of chromatogram peaks from direct sequencing, hence inosine is decoded as guanosine by the translation machinery (Barbon et al., 2003; Huang et al., 2012a). Accordingly, I examined whether A-to-I RNA editing levels are under circadian control. The editing level at the Q/R decoding site of *Flnb* (*Filamin beta*) and the Q/R decoding site of *Cdk13* (*Cyclin-dependent kinase 13*) showed robust changes in a circadian manner with peaks at CT 6-10 (Fig. 14). It was reported that ADAR2 edits its own pre-mRNA generating a new splice site for long isoform of *Adar2* mRNA, which has been used as a marker for the ADAR2 deaminase activity (Maas et al., 2001; Rueter et al., 1999) (Fig. 15A). I revealed the expression rhythm of the long isoform of *Adar2* transcripts by qRT-PCR with the isoform-specific primers, implying that the editing activity *per se* has rhythmicity (Fig. 15B). The relative band intensity from RT-PCR products of *Adar2* long isoform demonstrated consistent results (Fig. 15C). These editing events were kept at constantly low levels throughout the days in *Bmal1*-knockout mice liver (Fig. 14B, 15B; Middle), in which the *Adar2* expression rhythms were abolished (Fig. 12C). Then, I assessed the effects of ADAR2 on rhythmic editing events by using $Adar2^{-/-}$ / $Gria2^{R/R}$ mice, exhibiting complete loss of the editing events that were observed in the littermate $Adar2^{+/+}$ / $Gria2^{R/R}$ mice (Fig. 14B, 15B; Bottom). Note that the knock-in allele of $Gria2^{R/R}$ should not affect the circadian oscillation in mice liver, where *Gira2* gene does not express. These data demonstrated that the A-to-I RNA editing mediated by rhythmic *Adar2* showed circadian variation.

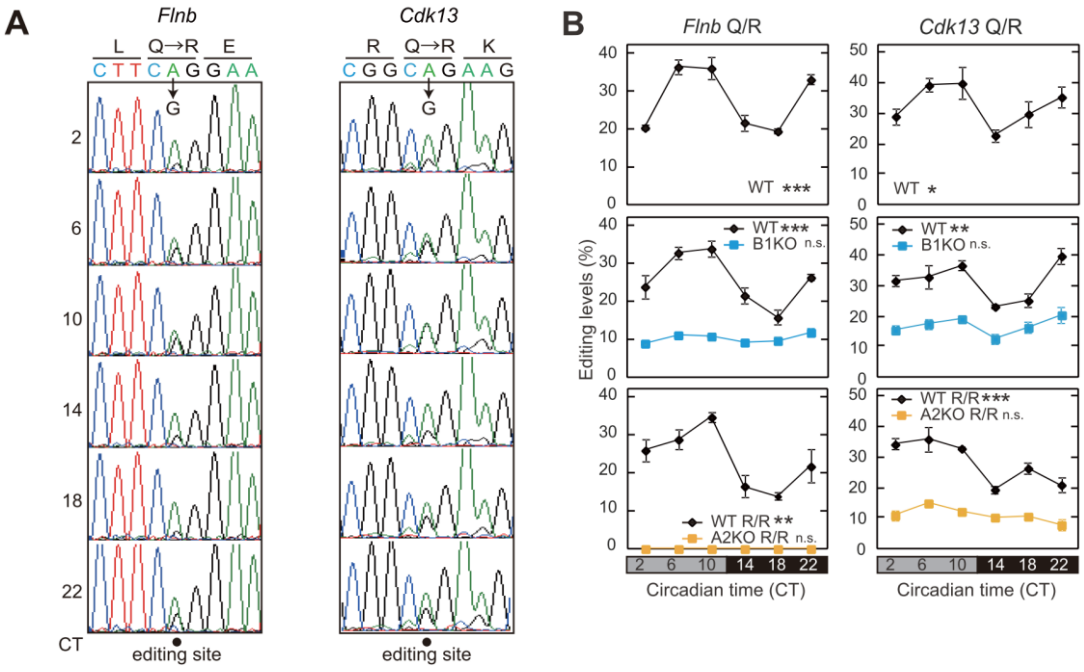

Figure 14　Determination of rhythmic editing levels regulated by *Adar2*

(A) Direct-sequencing chromatograms from RT-PCR products of *Flnb* and *Cdk13* transcripts.　Closed circles represent the decoding editing sites.　(B) Circadian profiles of editing level [G / (A+G) (%)] in *Flnb* and *Cdk13* transcripts showed rhythmical editing levels and attenuated or no editing with *Bmal1* or *Adar2*- deficient genotypes.　Change over time was analyzed by one-way ANOVA, * = $p < 0.05$, ** = $p < 0.01$, *** = $p < 0.001$, n.s. = $p \geqq 0.05$.　Data are means with SEM from three independent mice ($n = 3$).

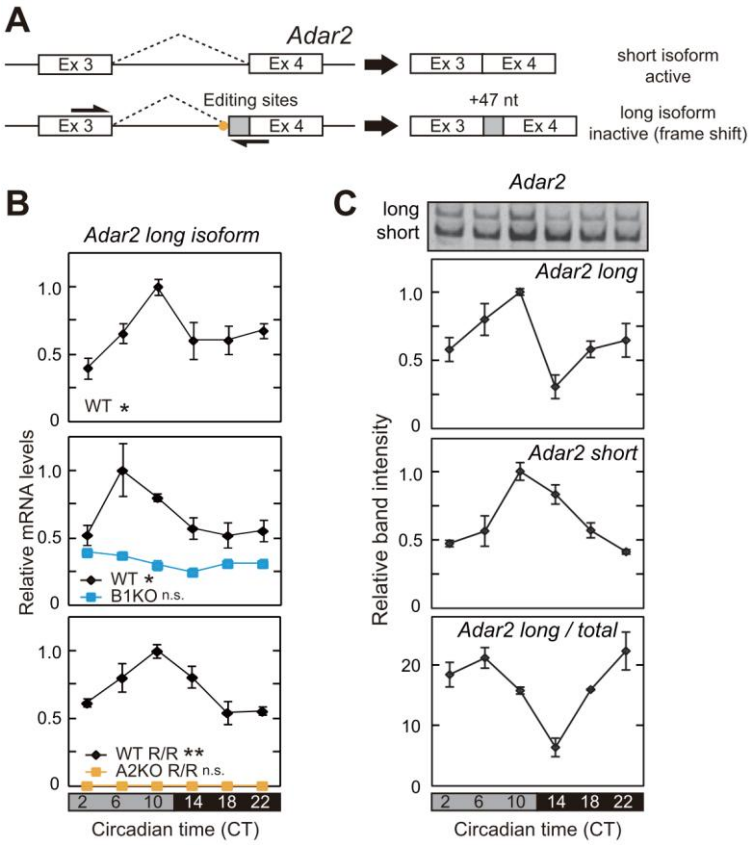

Figure 15　Circadian regulation of alternative splicing mediated by *Adar2* auto-editing

(A) Regulation of alternative splicing by ADAR2-mediated editing (Rueter et al., 1999). *Adar2* gene structural models at around an auto-editing site (shown as a yellow circle) and alternative splicing patterns are indicated.　Auto-editing creates a new splicing acceptor site and causes inclusion of the 47 nucleotides cassette (shown as a shaded box) to the mature *Adar2* transcript resulting in the expression of truncated inactive ADAR2 due to frame shift.　Inverted arrows indicate primers for qRT-PCR of the long isoform mRNA.　(B) Circadian expression profiles of long isoform of Adar2 transcripts in mouse liver quantified by qRT-PCR analysis.　The signals were normalized to Rps29 for each sample and the mean value at the peak time was set to 1. Data are means with SEM from three independent mice (n = 3).　Change over time was analyzed by one-way ANOVA, * = $p < 0.05$, ** = $p < 0.01$, n.s. = $p \geqq 0.05$.　(C) RT-PCR analyses for quantifying the efficiency of Adar2 auto-editing.　The PCR products corresponding to long isoforms and short isoforms of Adar2 transcripts are indicated and the relative band intensities are plotted.

3.3.3 Genome-wide identification of rhythmic RNA editing in mouse liver

To date, advances in sequencing technologies have identified a large number of A-to-I RNA editing sites in human and mouse, which were registered in the database of DARNED and RADAR (Kiran et al., 2012; Ramaswami and Li, 2014; Sakurai et al., 2014; Wulff et al., 2011). Hence, I employed RNA-Seq analysis to profile genome-wide circadian editing events in the *Adar2*-knockout (*Adar2*$^{-/-}$ / *Gria2*$^{R/R}$) and the wild-type littermates (*Gria2*$^{R/R}$) mice liver. Poly(A)+ RNAs were prepared from mice liver isolated 4 hr intervals under DD condition with two biological replicates at every time points, and were subjected to Illumina HiSeq^{TM} 2500 sequencing (paired end 101 bp reads). Raw sequence reads were aligned to the mouse genome (mm10) at most six mismatches. For quantification of editing level [G / (A+G) (%)], the number of aligned reads including A and G base at editing sites were enumerated. For instance, the editing level calculated from the sequenced reads at the Q/R decoding site of *Flnb* showed a robust change in a circadian manner (Fig. 16), which agreed very well with the direct sequencing result (Fig. 14B). No occurrence of G base was found at the editing site in the aligned reads of *Adar2*-knockout mice transcripts. Among the 8,410 registered editing sites in the DARNED and RADAR, 743 sites had more than 5-read coverage at every time points in our liver transcriptome data enough to determine their editing levels. The editing levels of 132 editing sites exhibited statistically significant rhythmicity in my dataset analyzed by CircWave ver3.3 (Oster et al., 2006) (Fig. 17A, Table 4). Large parts of them were found in 3'UTR region, and only 5 rhythmic editing sites were found in CDS (Fig. 17B). All of the rhythmic editing levels in CDS were examined by direct sequencing, and the rhythmic editing levels were completely abolished in the *Adar2*-knockout mice except for the *Azin1* editing sites (Fig. 18A). Futhermore, the rhythmic editing levels in 3'UTR and intronic region were validated by direct sequencing (Fig. 18B,

C). The peak phases of the rhythmic editing levels were largely at CT6-10, and the profiles of editing peak phases were altered by *Adar2*-deficinecy, suggesting the rhythmic editing events were mainly regulated by *Adar2* (Fig. 19). In fact, about 85% of rhythmic editing sites exhibited the attenuation of rhythmicity in the *Adar2*-knockout mice, and 60% exhibited no significant rhythmicity (Fig. 19A). Gene expression levels of the transcripts, in which the rhythmic editing sites were found, did not show distinct rhythmicity and their peak phases were not enriched at CT6-10 (Fig. 20). This result suggested that the turnover of transcripts should not be main attribution of the rhythmic editing levels. Collectively, the deep-sequencing analysis demonstrated the comprehensive circadian profiles of A-to-I RNA editing levels mainly attributed to *Adar2*.

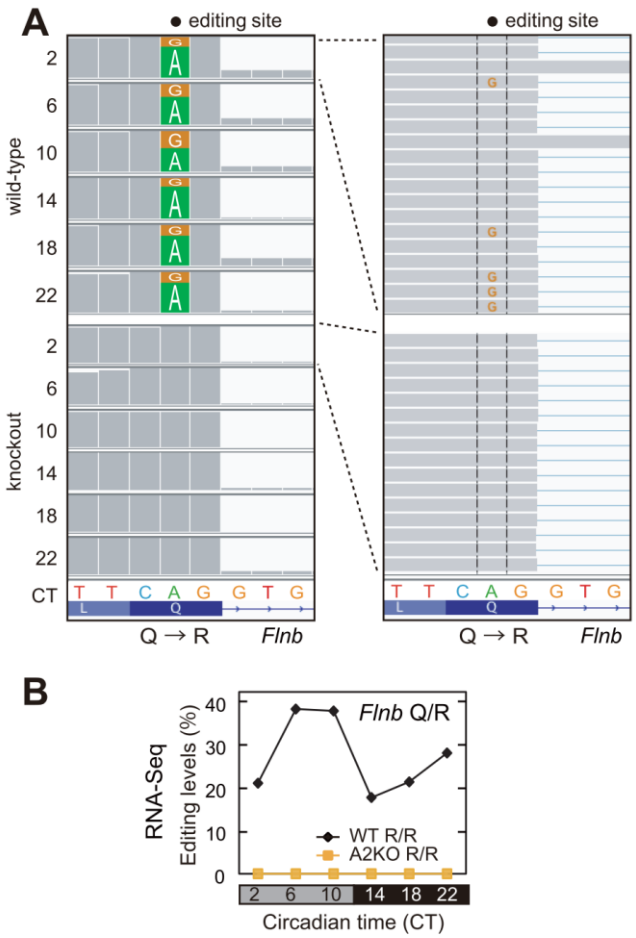

Figure 16　Calculation of the rhythmic editing level in the *Flnb* transcripts by RNA-Seq analysis

(A) Aligned sequenced tags at around the Q/R site of *Flnb* transcripts shown with the gene structure.　A Closed circle represents the editing site.　(B) Circadian profiles of editing level [G / (A+G) (%)] at the editing sites of *Flnb* transcripts in the *Adar2*-knockout mice (*Adar2*$^{-/-}$ / *Gria2*$^{R/R}$) and the wild-type littermates (*Adar2*$^{+/+}$ / *Gria2*$^{R/R}$) revealed by the number of aligned tags in RNA-Seq analysis

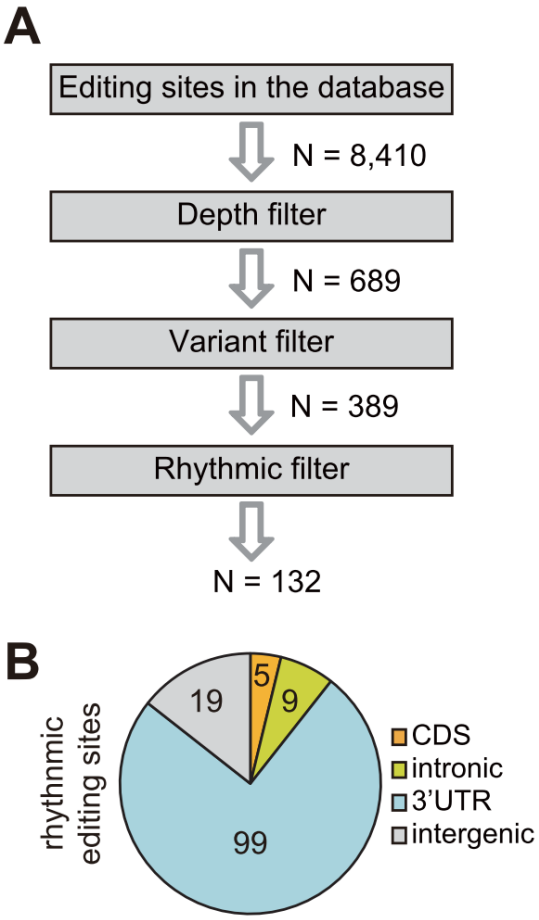

Figure 17 Identification of rhythmic editing sites by RNA-Seq analysis

(A) A flowchart for comprehensive identification of rhythmical editing sites. (B) A pie chart classifying the 132 rhythmic editing sites into categories based on their positions in the mouse genome.

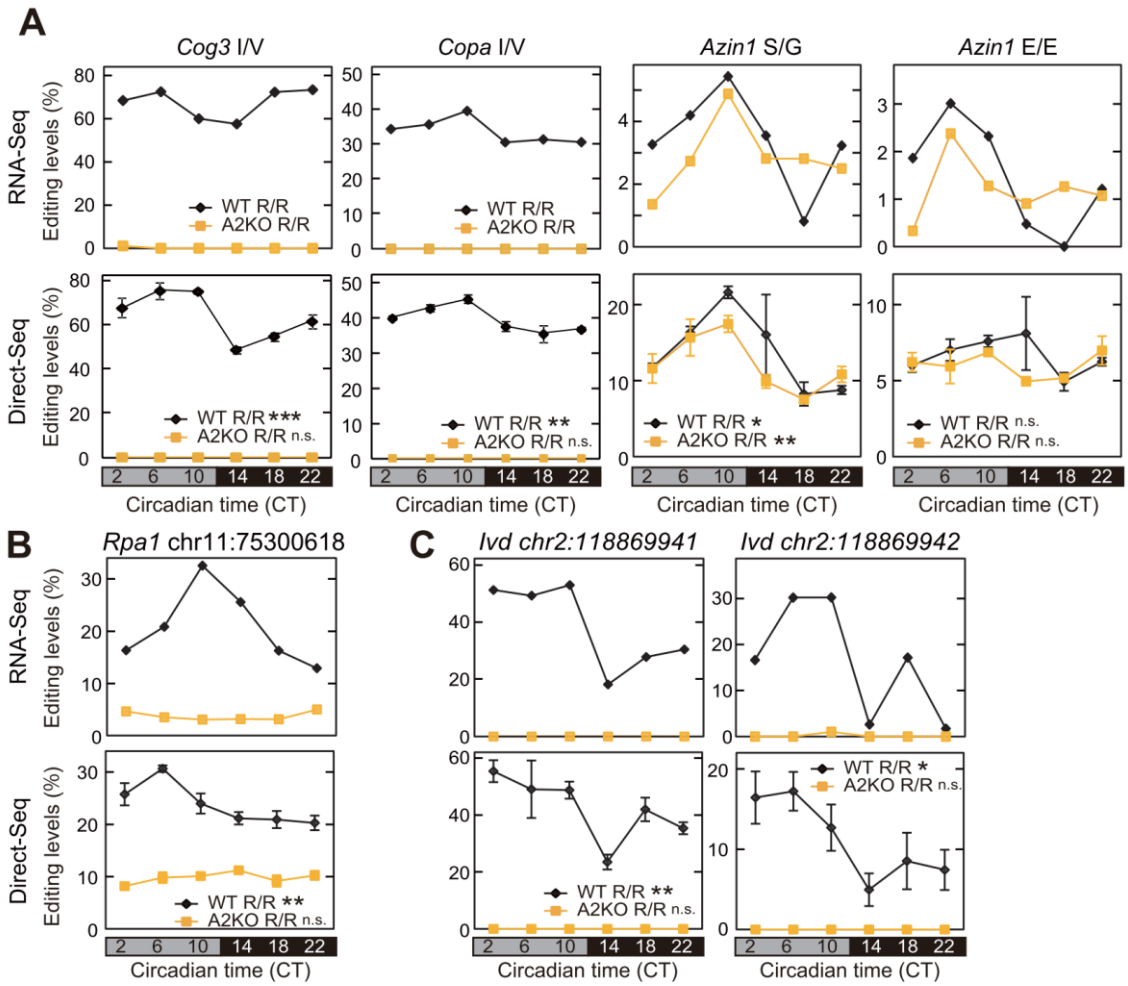

Figure 18　Rhythmic editing levels quantified by direct-sequencing

The circadian profiles of editing levels at the editing sites in CDS (A), in 3'UTR (B) and in intronic (C) region revealed by RNA-Seq (Top) and direct sequencing (Bottom). Change over time was analyzed by one-way ANOVA, * = $p < 0.05$, ** = $p < 0.01$, *** = $p < 0.001$, n.s. = $p \geqq 0.05$.

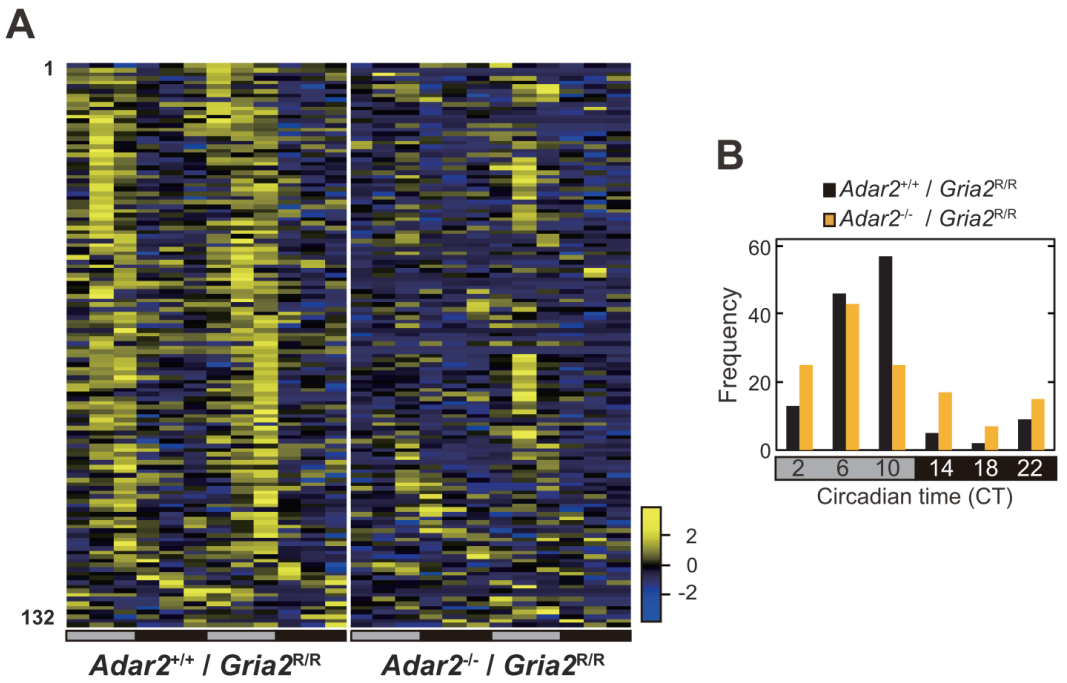

Figure 19 Circadian differences of editing levels at the rhythmic editing sites

(A) Heatmap representation of rhythmically regulated editing levels (n = 132). Editing levels of two biological replicates across time points in the *Adar2*-knockout (Left) and the littermates wild-type (Right) mice were shown in each lane corresponding to one editing site, ordered by the peak phases. High levels were displayed in yellow and low in blue. (B) The acrophase distribution of editing levels at the rhythmic editing sites.

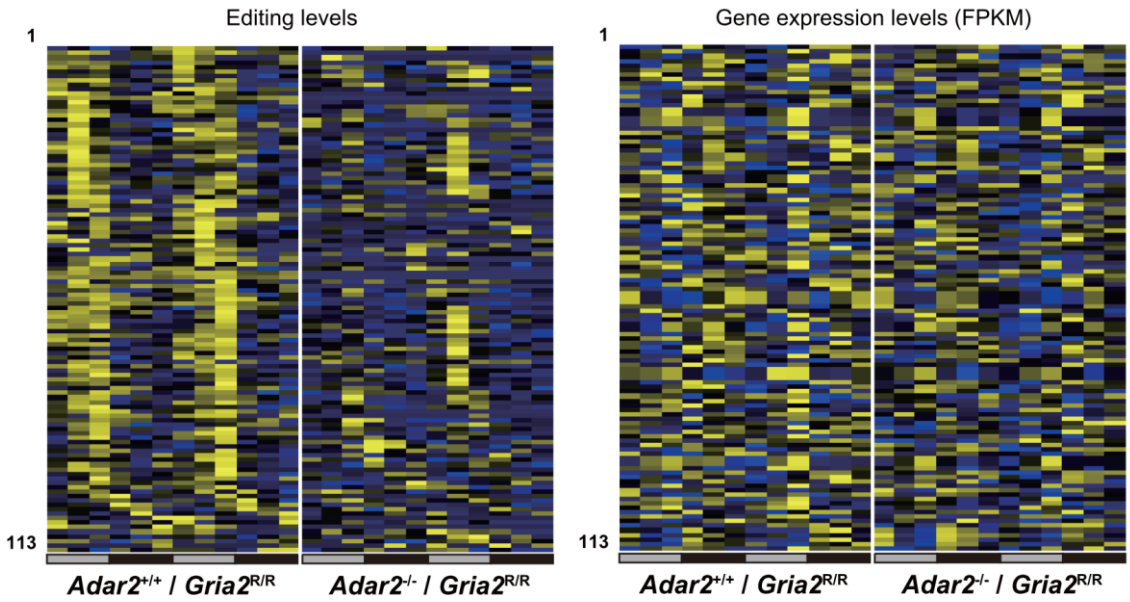

Figure 20 The correlation between the editing levels and the gene expression levels

Heatmap representation of rhythmic editing levels which were located in the annotated transcripts (*n* = 113, Left) and the gene expression levels (*n* = 113, Right) correspond to the transcripts attributed to the rhythmic editing sites. Editing levels of two biological replicates across time points were shown in each lane corresponding to one editing site, ordered by the peak phases.

3.3.4 *Adar2* affects the circadian period in gene expression rhythm and wheel-running rhythm

To confirm these editing rhythms were not caused by attenuation of circadian oscillation in the *Adar2*-deficient state, I analyzed circadian gene expression. For the estimation of RNA expression levels, Fragments Per Kilobase of exon per Million mapped fragments (FPKM) were calculated by using Cufflinks version 2.2.1 (Trapnell et al., 2010). Expression levels of all transcripts were estimated and showed high reproducibility between replicate samples with average R^2 values 0.98 (Fig. 21A). Core clock genes were rhythmic in both genotype mice, which was consistent with qRT-PCR data, indicating highly quantitative analysis of my RNA-Seq dataset (Fig. 21B, C). Intriguingly, the expression profiles of core clock genes in the *Adar2*-knockout mice were found to be phase-advanced rhythm when compared to the wild-type littermates (Fig. 21C). In addition, 659 transcripts (4.9% of expressed genes) that were identified as rhythmic in both genotype mice (Fig. 22A, see Methods) exhibited statistically short period and phase-advanced rhythm in the knockout mice (Fig. 22B, C). The frequency distribution of the peak phases also showed phase advances (Fig. 22D). These data raise the possibility that *Adar2* affects the periodicity of circadian oscillation.

Short hairpin RNAs (shRNAs) against *Adar2* reduced the endogenous mRNA levels of *Adar2* and inhibited the expression of Flag-ADAR2 protein in NIH3T3 cells (Fig. 23A, B). The knockdown and overexpression of *Adar2*, which caused down- and up-regulation of the A-to-I RNA editing activity (Fig. 23C), respectively, shortened and lengthened the period of the cellular clock (Fig. 24). In order to definitively evaluate the physiological function of *Adar2* in determination of circadian period *in vivo*, the locomotor activities of $Adar2^{-/-}$ / $Gria2^{R/R}$, $Adar2^{+/+}$ / $Gria2^{R/R}$ and $Adar2^{+/+}$ / $Gria2^{Q/Q}$ mice were recorded under DD conditions after two weeks entrainment in the 12-h-

light/12-h-dark (LD) cycle (Fig. 25A). *Adar2*$^{-/-}$ / *Gria2*$^{R/R}$ mice exhibited rhythmic activities with a free-running period (τ_{DD}) of 23.54 ± 0.04 hr, which was significantly shorter than that of their control littermates (*Adar2*$^{+/+}$ / *Gria2*$^{R/R}$ τ_{DD}: 23.76 ± 0.03 hr) (Fig. 25B). This short period phenotype was consistent with the gene expression rhythms from my transcriptome data and cellular rhythms (Fig. 22, 24). No significant change in circadian periodicity between *Adar2*$^{+/+}$ / *Gria2*$^{R/R}$ and *Adar2*$^{+/+}$ / *Gria2*$^{Q/Q}$ mice indicated that the knock-in allele of *Gria2*$^{R/R}$ would not affect the circadian periodicity of the wheel-running rhythm (Fig. 25B). In the eight-hour jet-lag experiments, the *Adar2*-knockout mice showed significantly faster re-entrainment to the new advanced LD schedule compared to the control littermates (Fig. 26A, B). Re-entrainment to the delayed LD cycles showed statistically no difference between the two genotypes (Fig. 26C). The profiles of the activity onset also exhibited that the *Adar2*-knockout mice entrained to the delayed LD cycles more rapidly than the control littermates (Fig. 26D). The immediate re-entrainment to phase-advanced LD cycles were probably caused by the short periodicity, reinforcing the short period phenotype of the *Adar2*-knockout mice. Notably, in the previous studies, the gene expression profiles in the SCN with a nocturnal light pulse stimulation did not show a distinct change in *Adar2* expression, indicating that light did not appear to influence Adar2 expression in the SCN (Hatori et al., 2014; Jagannath et al., 2013).

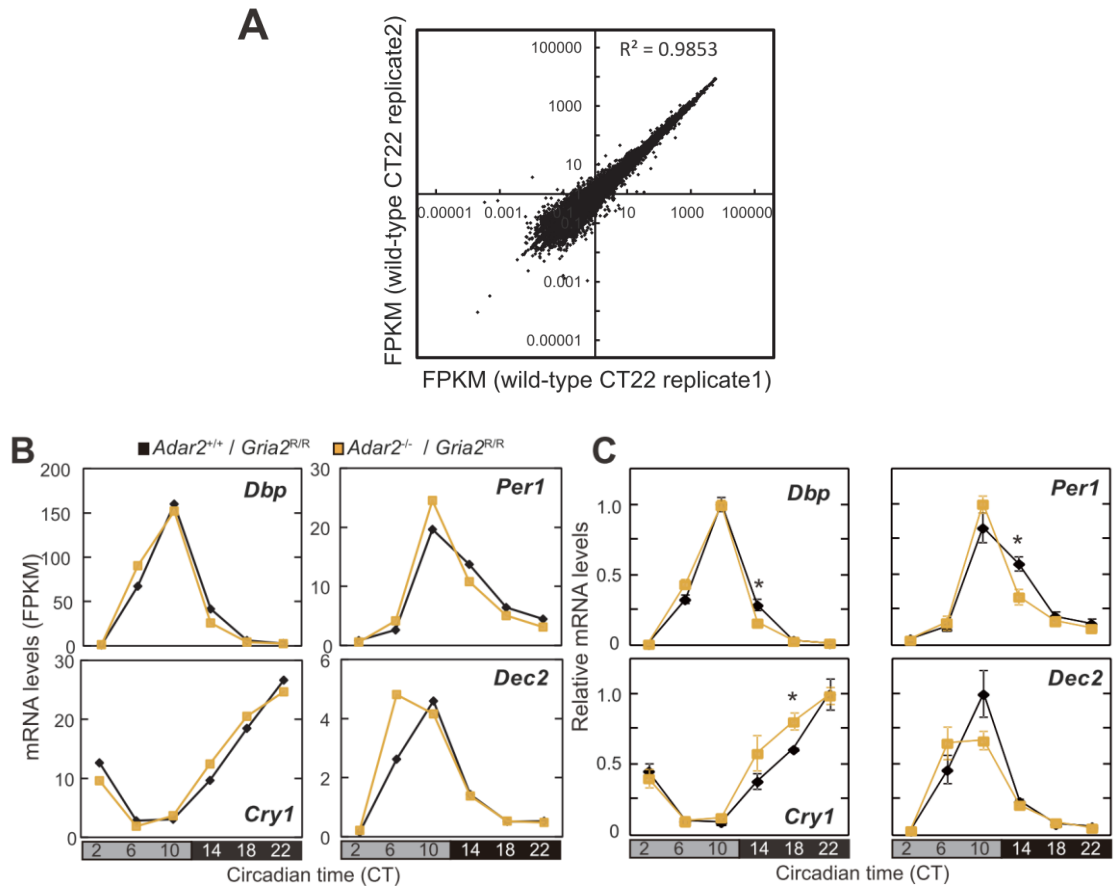

Figure 21 The expression rhythms of core clock genes in the *Adar2*-knockout mice

(A) Comparison between the biological replicates of transcript expression levels (FPKM) exhibited a high degree of reproducibility with average R^2 values 0.98. The expression levels per gene were plotted. (B and C) Circadian expression profiles of typical core clock genes in the *Adar2*-knockout mice (*Adar2*$^{-/-}$ / *Gria2*$^{R/R}$) and the wild-type littermates (*Adar2*$^{+/+}$ / *Gria2*$^{R/R}$) are revealed by RNA-Seq analysis (B) and by qRT-PCR analysis (C). In panel (C), The signals were normalized to Rps29 for each sample and the mean value at the peak time was set to 1. Data are means with SEM from three independent mice (n = 3). Difference between the genotypes were analyzed by Student's t-test, * = $p < 0.05$.

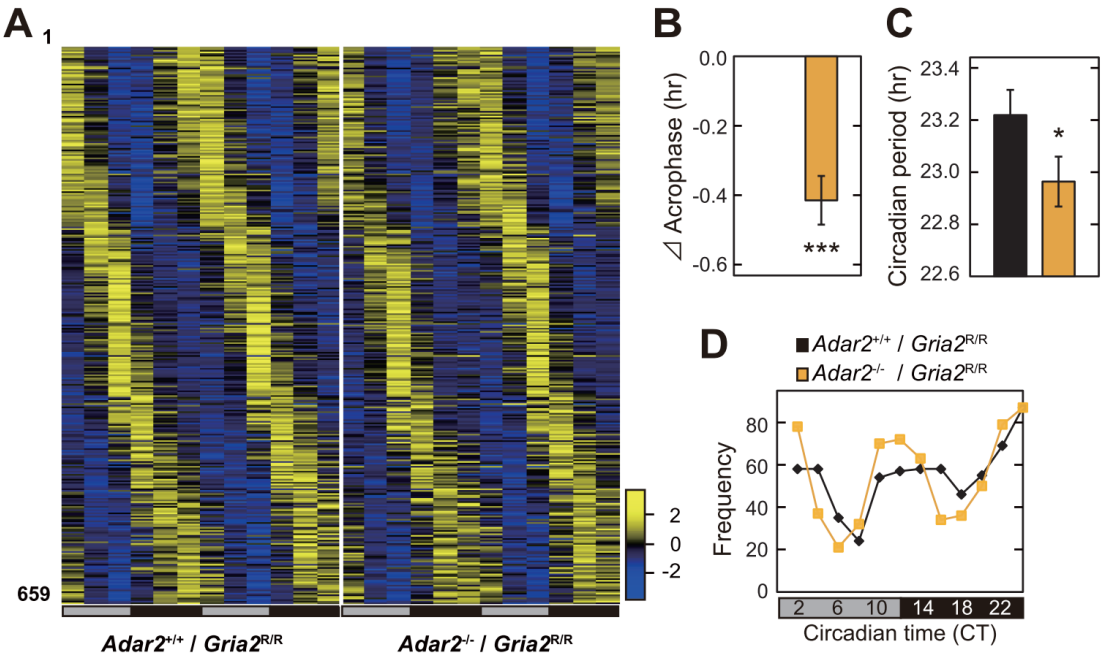

Figure 22 Comprehensive analysis for gene expression rhythms revealed by RNA-Seq in the *Adar2*-knockout mice

(A) Heatmap representation of the rhythmically expressed genes both in the *Adar2*-knockout mice and the wild-type littermates (n = 659). Gene expression levels of two biological replicates across time points were shown in each lane corresponding to one gene, ordered by the phases. High expression was displayed in yellow and low expression in blue. (B and C) A difference of circadian peak phases (Δacrophase) (B) and circadian periods (C) of gene expression rhythms between the genotypes (n = 659; * = $p < 0.05$, *** = $p < 0.001$ by Paired t-test). The period and phase from Circwave were used for the analysis. The acrophase of each genes in the wild-type was set to 0 in (B). (D) The acrophase distribution of rhythmic genes in both genotypes.

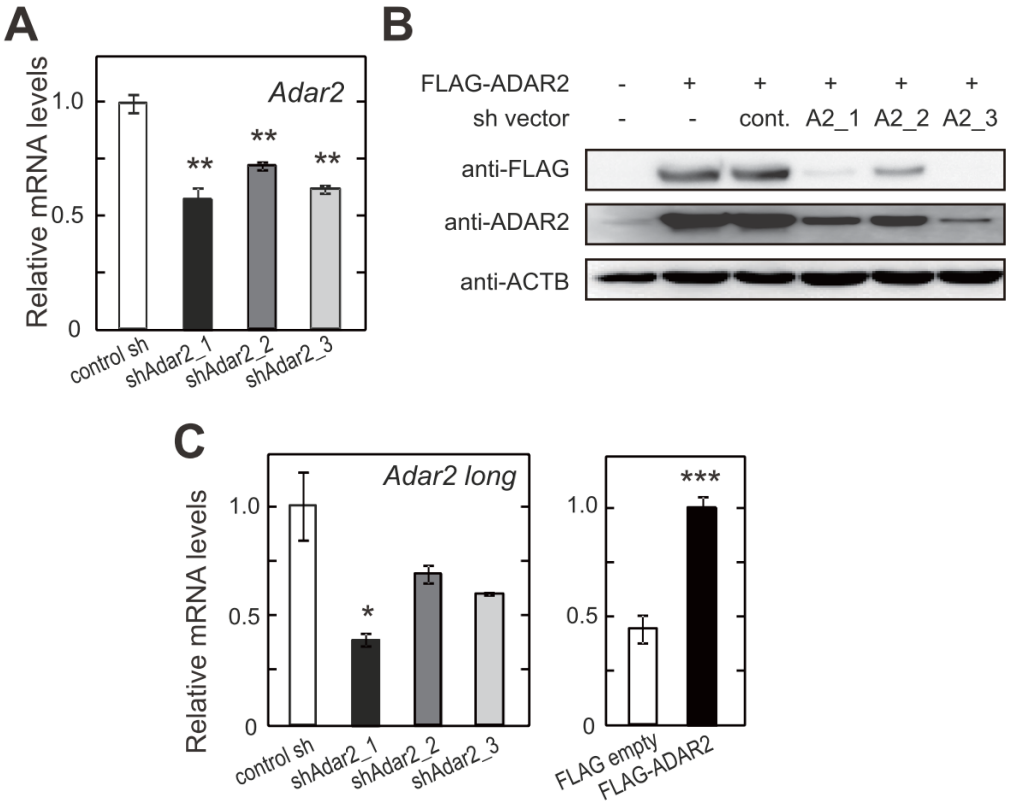

Figure 23 Knockdown and overexpression of *Adar2* in NIH3T3 cells

(A) Unsynchronized NIH3T3 cells were transiently transfected with shRNA expression vectors (shAdar2_1, shAdar2_2 and shAdar2_3) for *Adar2* and its transcripts were measured by qRT-PCR. The signals were normalized to Rps29 for each sample and the mean value of control shRNA induced cells was set to 1. Data are means with SEM from three independent experiments (n = 3). (B) Unsynchronized NIH3T3 cells were transiently transfected with a Flag-ADAR2 expression vector in combination with an *Adar2* shRNA or control shRNA expression vector. The cell lysates were subjected to immunoblotting. ACTB served as a loading control. (C) Expression levels of the long isoforms of Adar2 in NIH3T3 cells transfected with *Adar2* shRNA expression vectors or a Flag-ADAR2 expression vector. Statistics and abbreviations as in (A).

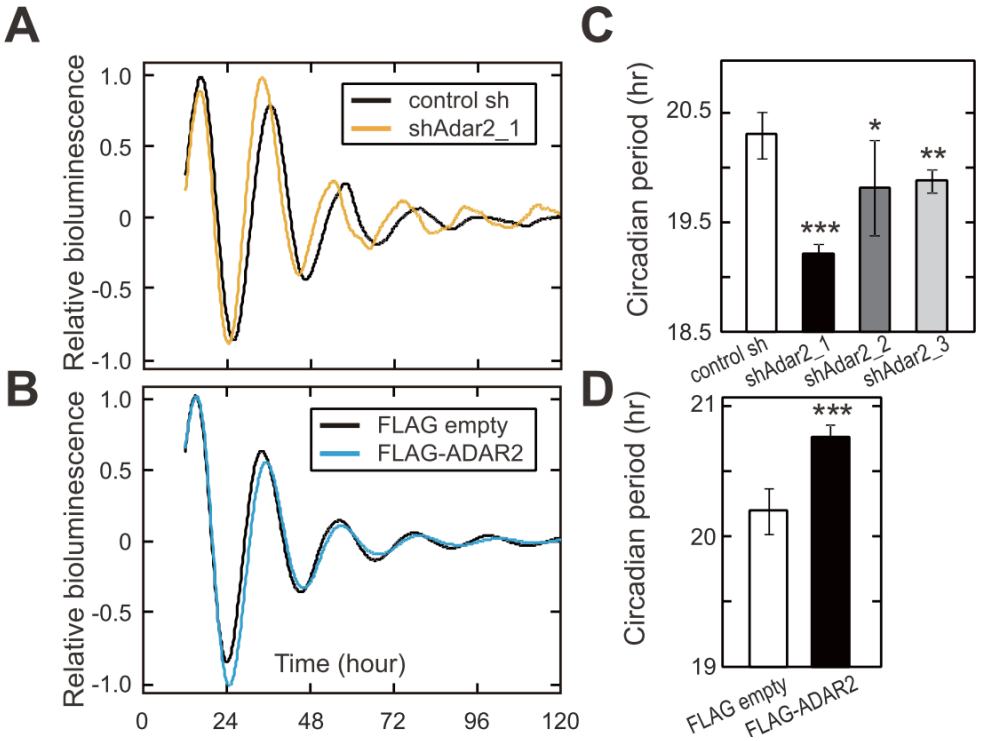

Figure 24 Cellular rhythms of *Adar2* knockdown and overexpression cells

(A and B) NIH3T3 cells were transiently transfected with a *Bmal1*-luciferase reporter in combination with an *Adar2* shRNA (A) or a Flag-ADAR2 (B) expression vector. Twenty-four hours after transfection, the cells were synchronized with dexamethasone treatment for 2 h, and luciferase activity was monitored. A representative set of bioluminescence rhythms is shown. (C and D) The period length of bioluminescence rhythm in panels (A and B) is shown. Data are means with SEM (n = 6; (A), n= 8; (B), * = $p < 0.05$, ** = $p < 0.01$, *** = $p < 0.001$ by Student's t-test, versus control shRNA or Flag empty).

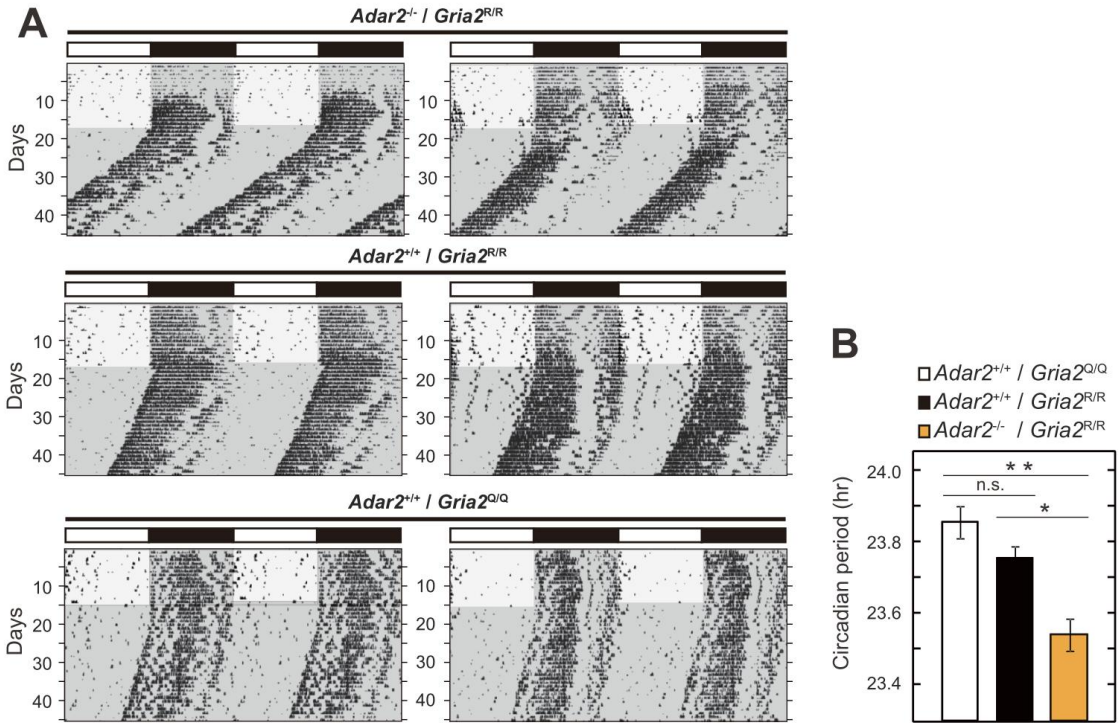

Figure 25　Wheel-Running Activities of the *Adar2*-knockout Mice

(A) Representative double-plotted actograms of the wheel-running activities of three genotypes.　Mice were entrained to LD cycle for at least 2 weeks and subsequently transferred to DD conditions.　Dot plots represent wheel running activity, and gray shading indicates dark lighting conditions.　(B) Circadian periods of free-running activities in DD determined by chi-square periodogram.　Data from days 11 through 24 in DD were used for the calculation of the circadian periods.　Data are means with SEM (n = 12 ($Adar2^{+/+}$ / $Gria2^{Q/Q}$), 14 ($Adar2^{+/+}$ / $Gria2^{R/R}$) and 21 ($Adar2^{-/-}$ / $Gria2^{R/R}$); * = $p < 0.05$, ** = $p < 0.01$, n.s. = $p \geqq 0.05$ by Tukey‐Kramer method).

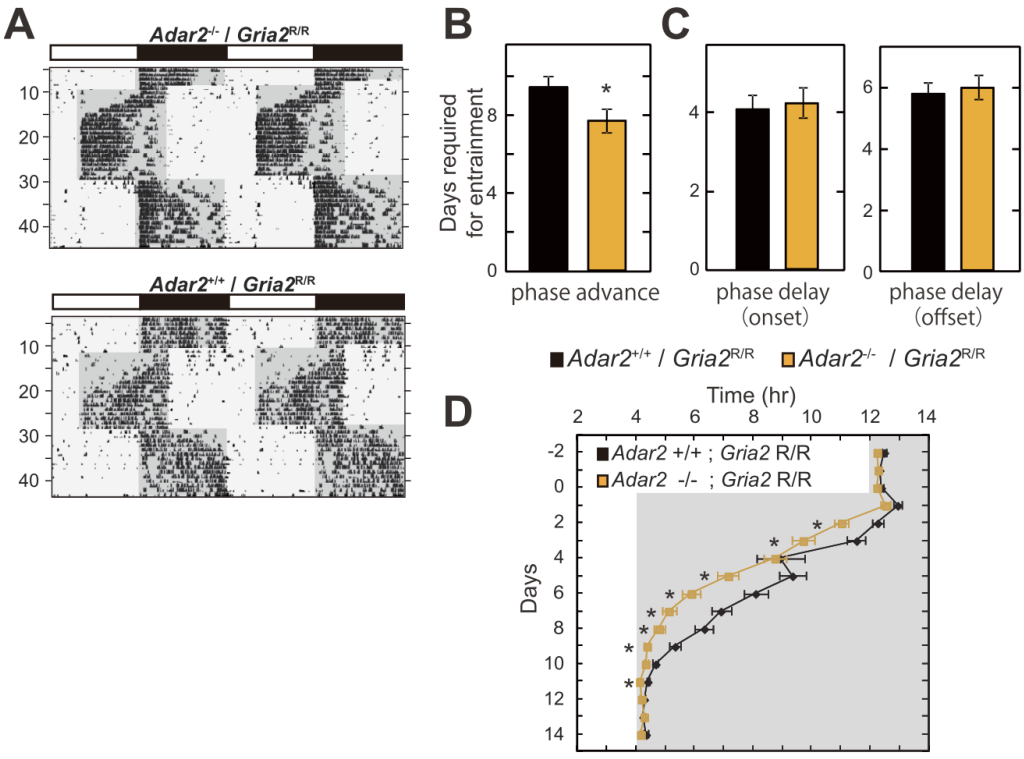

Figure 26 Jet lag experiments of the *Adar2*-knockout mice

(A) Representative double-plotted actograms of the wheel-running activities of 8 hr LD phase advance and subsequently 8 hr LD phase delay. (B and C) Days required for re-entrainment to 8 hr advanced (B) and 8 hr delayd (C) LD cycles. Data are means with SEM (n = 15 ($Adar2^{+/+}$ / $Gria2^{R/R}$) and 17 ($Adar2^{-/-}$ / $Gria2^{R/R}$) for advanced LD cycles, and n = 13 ($Adar2^{+/+}$ / $Gria2^{R/R}$) and 12 ($Adar2^{-/-}$ / $Gria2^{R/R}$) for delayed LD cycles; * = $p < 0.05$ by Student's t test). (D) The time of activity onset during 8 hr advanced jet-lag conditions was determined by ClockLab software. The means of the onset times were plotted with error bars indicating SEM (* = $p < 0.05$ by Student's t test).

3.3.5 *Adar2* modulates the circadian period *via* miRNA-mediated silencing of *Cry2* translation

Such a short-period phenotype should be caused by altered expression of clock components, I investigated the circadian profiles of core clock proteins CRY1, CRY2, PER2, CLOCK and BMAL1 in the Adar2-knockout mice liver (Fig. 27A, B). CRY2 protein significantly increased at CT14-18, whereas *Cry2* mRNA level did not change at any time points, suggesting the miRNA-mediated translational regulation of *Cry2* (Fig. 27B, C). It is well known mechanism that ADAR enzymes regulate miRNA biogenesis, since miRNAs are produced from a precursor transcripts harboring a double-stranded stem-loop structure, which can serve as a substrate for ADARs (Nishikura, 2010). Importantly, the miRNA-mediated gene silencing of *Cry2* were previously reported (Du et al., 2014), and the programs for miRNA target prediction, TargetScan (Garcia et al., 2011) (http://www.targetscan.org/) and miRNA.org (Betel et al., 2008) (http://www.microrna.org/microrna/home.do), predicted *Cry2* to be one of the targets of let-7g. The A-to-I RNA editing site in *pri-let-7g* transcript was reported (Kawahara et al., 2008). Furthermore, the previous study revealed that expression levels of mature let-7g were down-regulated in the *Adar2*-knockout mice, probably caused by the regulation of miRNA biogenesis by A-to-I RNA editing (Kawahara et al., 2007a; Vesely et al., 2012). Indeed, I found the attenuation of rhythmic profiles of *pri-let-7g* by *Adar2*-deficiency (Fig. 28A). Note that the circadian profiles of mature let-7g were shown in the published miRNA transcriptome analysis (Vollmers et al., 2012). In NIH3T3 cells, knockdown of *Adar2* significantly up-regulated the activity of luciferase reporter harboring the *Cry2* 3' UTR, and this up-regulation of the reporter activity was completely abolished by introducing a mutation at the predicted let-7g target site in the *Cry2* 3' UTR (Fig. 28B). These experiments suggested a hypothesis mechanism that CRY2 protein

expression was suppressed by *Adar2* through the regulation of let-7g biogenesis, and the CRY2 accumulation should result in the short-period phenotype.

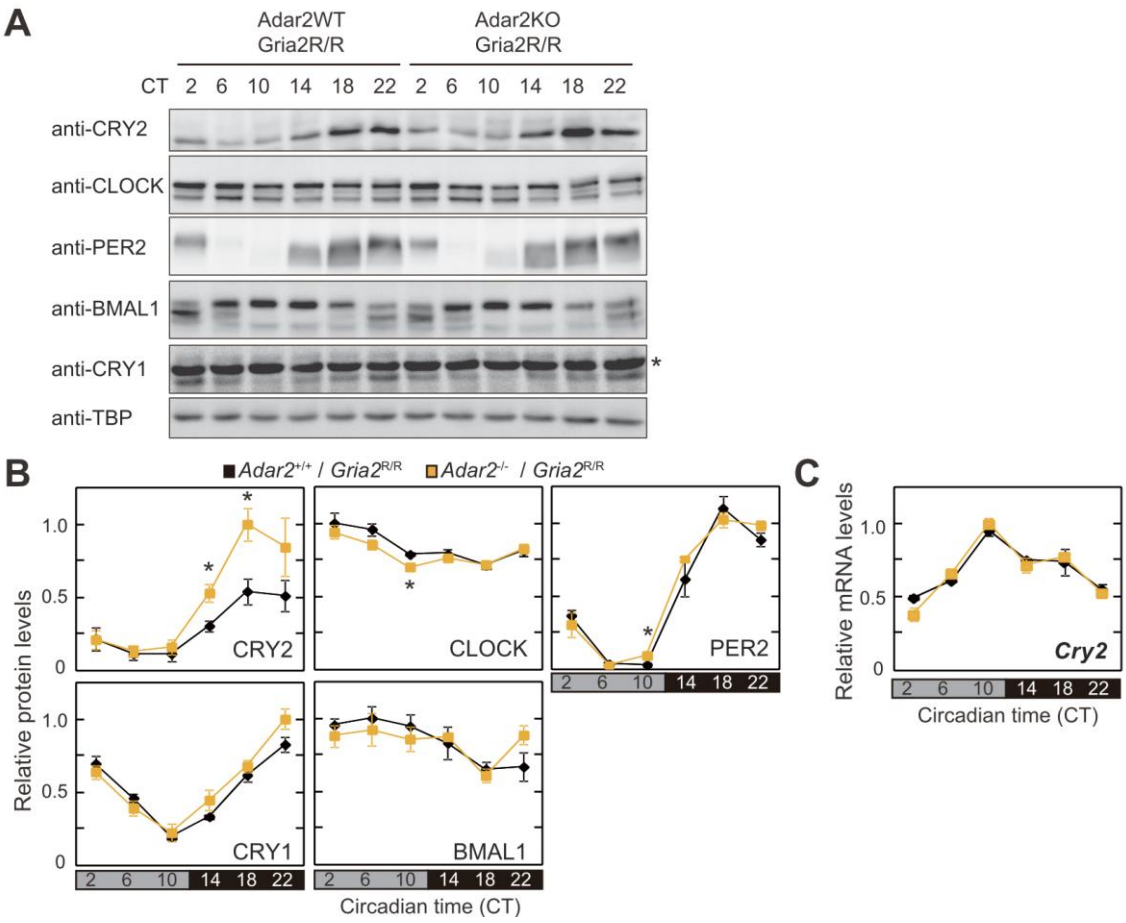

Figure 27 Circadian expression profiles of core clock genes in the *Adar2*-knockout mice

(A) Circadian expression profiles of CLOCK, BMAL1, CRY1, CRY2 and PER2 proteins in the Adar2-knockout mice and the wild-type littermates liver. A nonspecific band is indicated by an asterisk. TBP served as a loading control (bottom panel). (B) The band intensities in panels (A) were plotted. The signals were averaged from three independent mice and the mean value at the peak time was set to 1. Data are means with SEM (n = 3). Difference between genotypes were analyzed by Student's t-test, * = $p < 0.05$.

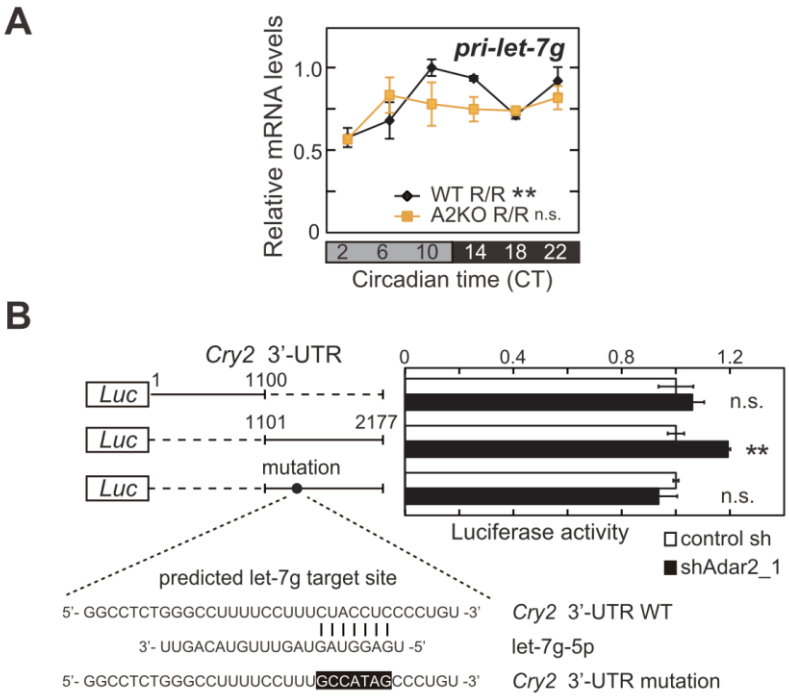

Figure 28　Post-transcriptional regulation of CRY2 by miRNA-mediated gene silencing

(A) Circadian expression profiles of *pri-let-7g* revealed by qRT-PCR.　The signals were normalized to Rps29 (mean ± SEM; $n = 3$).　Statistics and abbreviations as in Fig. 18.　(B) Dual luciferase assay of unsynchronized NIH3T3 cells transiently transfected with a luciferase-Cry2 3'UTR reporter (nt 1-1100 or 1101-2177) in combination with an Adar2 shRNA expression plasmid (mean ± SEM; $n = 3$; ** = $p < 0.01$, n.s. = $p \geqq 0.05$ by Student's t-test, versus control shRNA).　A mutation in the predicted let-7g target sites (nt 1369-1375) was shown as a black circle.

3.3.6 Adar2 post-transcriptionally regulates circadian outputs of various genes

A-to-I RNA editing modulates steady-state RNA levels through various mechanisms such as the regulation of miRNA biogenesis and the cleavage of hyper-edited dsRNA containing inosines (Kawahara et al., 2007b; Scadden, 2005). Indeed, a global effect of editing on expression levels of target RNAs was reported (St Laurent et al., 2013). A computational method, Cuffdiff (Trapnell et al., 2010), detected statistically significant changes in expression of transcripts between the genotypes, and the number of differentially expressed genes was changed across the time points with a peak at CT10 (Fig. 29A). The editing frequencies also showed rhythmic profiles with a peak at CT6-10 (Fig. 19), implying that *Adar2* rhythmically regulates the steady-state levels of the transcripts. To my surprise, a large fraction of genes identified as rhythmic in the *Adar2*-knockout mice were not overlapped with those in the wild-type mice (Fig. 29B). Among them, 359 genes (21% of rhythmic) were faithfully identified as rhythmic in the wild-type but not in the *Adar2*-knockout with statistical analysis by the three programs; JTK cycle, ARSER, Circwave (Fig. 30A, see Methods). I confirmed the rhythmic profiles of *Slco1a4* and *Aim1l* transcripts were actually attenuated in *Adar2*-deficient mice by qRT-PCR (Fig. 30B). On the other hand, 149 genes exhibited statistically significant rhythmicity in the *Adar2*-knockout but not in the wild-type (Fig. 31A). In fact, the rhythmic profiles of *Ugt2b38* transcripts were abolished by *Adar2*-deficiency (Fig. 31B), proposing a hypothetical mechanism of an *Adar2*-mediated homeostatic process that suppresses mRNA abundance rhythms of rhythmically transcribed genes in a tissue-specific manner. 359 transcripts, which were identified as rhythmic in the wild-type but not in the *Adar2*-knockout, did not largely have distinct transcription rhythms from the nascent RNA-Seq dataset, suggesting the important roles of *Adar2* on post-transcriptionally regulated RNA rhythms in mouse liver (Menet et al., 2012) (Fig. 32).

These experiments suggested that cyclic profiles of various RNA levels were post-transcriptionally produced by *Adar2*.

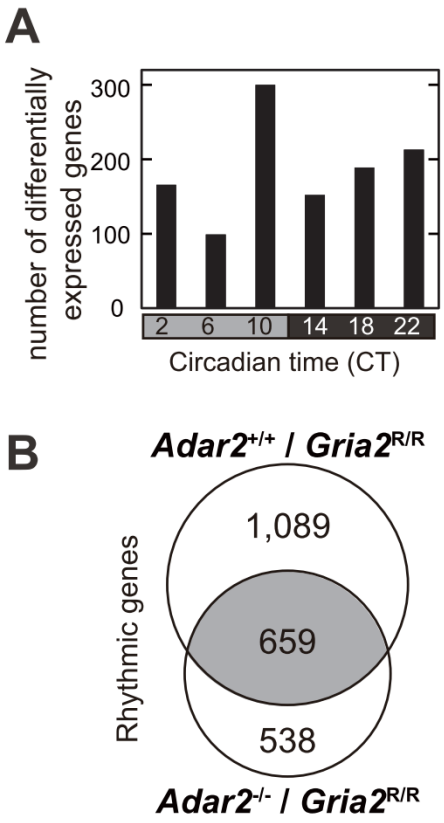

Figure 29 Gene expression profiles revealed by RNA-Seq

(A) The number of differentially expressed genes between the *Adar2*-knockout mice and the wild-type littermates liver (Cuffdiff; $q < 0.2$). (B) Overlap of rhythmic genes in the *Adar2*-knockout mice and the wild-type littermates.

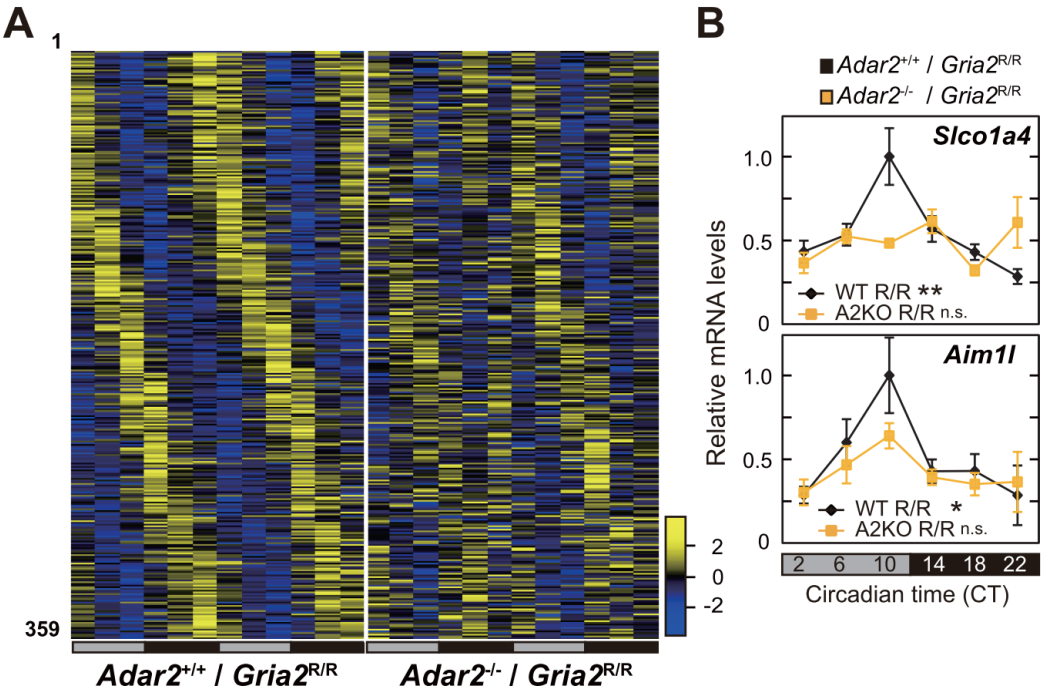

Figure 30 Cycling profiles of steady-state mRNA levels in the *Adar2*-knockout mice

(A) Heatmap representation of rhythmically expressed genes in the wild-type mice but not in the *Adar2*-knockout mice (n = 359). Gene expression levels of two biological replicates across time points were shown in each lane corresponding to one gene, ordered by the peak phases. (B) Circadian expression profiles of *Slcola4* and *Aim1l* revealed by qRT-PCR analysis. The signals were normalized to *Rps29* (mean ± SEM; n = 3). Statistics and abbreviations as in Fig. 18.

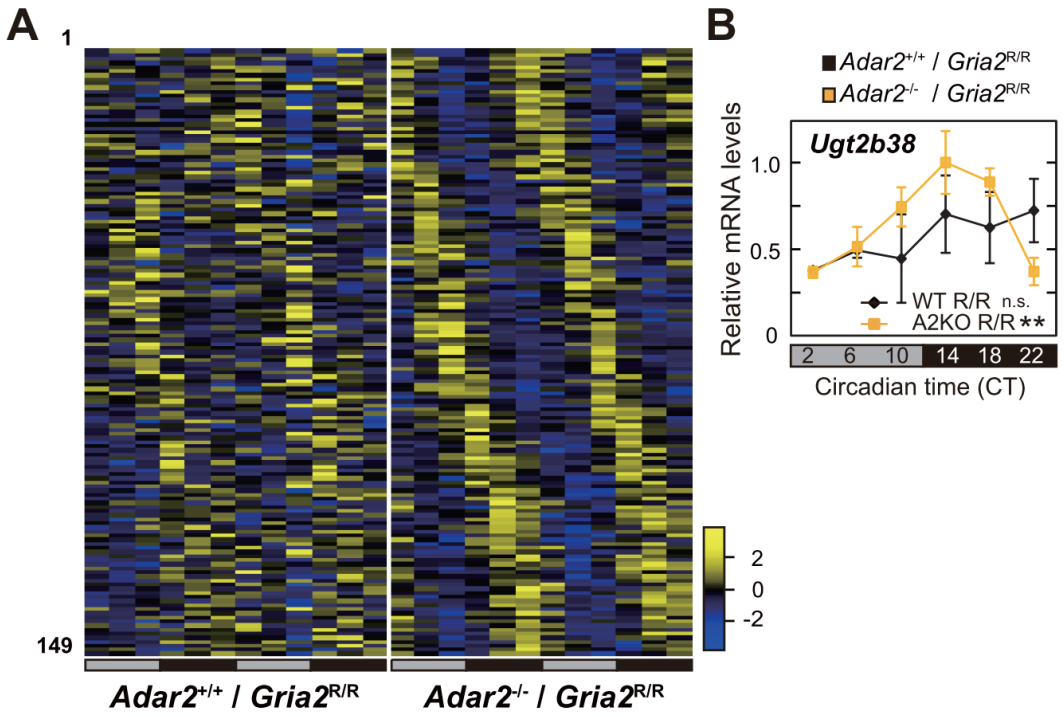

Figure 31 Cycling profiles of steady-state mRNA levels in the *Adar2*-knockout mice

(A) Heatmap representation of rhythmically expressed genes in the *Adar2*-knockout mice but not in the wild-type mice (n = 149). Gene expression levels of two biological replicates across time points were shown in each lane corresponding to one gene, ordered by the peak phases. (B) Circadian expression profiles of *Ugt2b38* revealed by qRT-PCR analysis. The signals were normalized to *Rps29* (mean ± SEM; n = 3). Statistics and abbreviations as in Fig. 18.

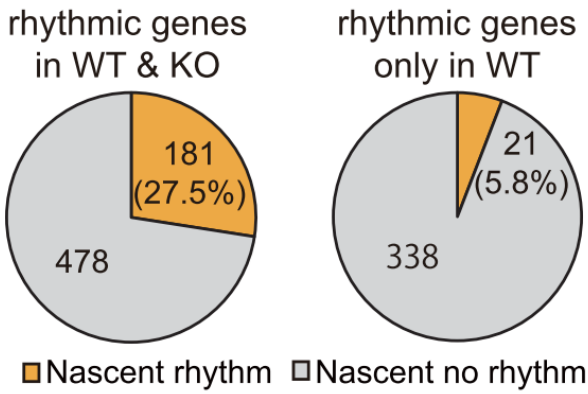

Figure 32 Gene transcription rhythms in the *Adar2*-knockout mice

Pie charts showing the distribution of gene transcription rhythms modified from Nascent RNA-Seq dataset in Menet *et al.* (Menet et al., 2012).

3.4 Discussion

Recent studies revealed that the post-transcriptional regulations such as RNA methylation, alternative splicing, polyadenylation, and miRNA-mediated gene silencing were rhythmically regulated by circadian clock, and they were also found to be important players in the modulation of circadian systems (Chen et al., 2013; Du et al., 2014; Fustin et al., 2013; Kojima et al., 2012; McGlincy et al., 2012). In the present study, I established the molecular and physiological link between circadian rhythm and A-to-I RNA editing for the first time in mammals. CLOCK and BMAL1 complex rhythmically binds to the promoter regions of *Adar2* gene locus and promotes *Adar2* expression rhythm (Fig. 12). Phase delay in *Adar2* expression between mRNA and protein would be caused by a negative auto-regulatory mechanism that the self-editing of *Adar2* mRNA results in a frameshift, producing a small non-functional protein (Fig. 15A). In the accumulating phase of *Adar2* mRNA expression and editing levels, ADAR2 protein expression was suppressed by auto-regulation. On the other hand, in the declining phase of editing activity, steady-state level of ADAR2 protein was gradually increased, and subsequently, ADAR2 produce next cycles of editing rhythms.

Constant and moderate low levels of *Adar2* in *Bmal1*-knockout mouse liver consequently resulted in arrhythmic and low editing activity profiles (Fig. 12C, 14B, 15B). In addition, *Adar2* deficiency caused complete loss of editing activities (Fig. 14B, 15B). These results strongly suggested that rhythmically expressed *Adar2* produces the rhythms of editing levels at various editing sites. Such rhythmic editing events at CDS regions probably cause circadian variations of protein functions. However, the physiological function of these rhythmical recoding events remained to be elucidated since the biological functions of these editing sites have been still elusive. I found that the

introduced Q to R substitution in the *Cdk13* proteins engender the putative nuclear localization signals (RQKRRR to RRKRRR) (Westergaard et al., 2010), raising the possibility that a rhythmical editing at this site could change localization of CDK13 protein in a circadian manner.

I extensively analyzed how *Adar2* affects the editing levels and gene expression rhythms by using deep-sequencing. *Adar2* has a large effect on editing level rhythms and gene expression profiles. My analysis revealed the surprising results that the cycling profiles of approximate 20% of all rhythmic genes depended on *Adar2*-mediated post-transcriptional regulation. Recently, RNA-Seq and Nascent-Seq experiments in mouse liver have demonstrated that a large fraction of steady-state mRNA levels that have rhythms are not transcribed rhythmically (Koike et al., 2012; Menet et al., 2012). My experiments elucidated that A-to-I RNA editing constitutes a part of mechanisms that produce the oscillation of stady-state mRNA levels without transcriptional rhythm. Precisely what aspects of *Adar2*-dependent events produce the rhythms of steady-state mRNA levels have remained unclear, however, the present study indicates one possible mechanism that *Adar2* rhythmically regulates the biogenesis of miRNAs which regulate gene expression rhythms.

Previous reports described that $Adar2^{-/-}$ / $Gria2^{R/R}$ mice display normal appearance and life span, and the physiological role of all ADAR2 substrates had remained to be elucidated except for limited numbers of targets especially in central nervous system (CNS). Present RNA-Seq data revealed that the expression profiles of various clock-controlled genes in the *Adar2*-knockout mice liver exhibited significantly short-period rhythms compared to the wild-type littermates, which is consistent with the short-period phenotypes of behavioral experiments (Fig. 25, 26). Short-period phenotype of the *Adar2*-knockout mice were attributed to up-regulation of CRY2 protein by the loss of

miRNA-mediated translational repression caused by *Adar2*-mediated miRNA biogenesis. Consistently, the previous study revealed the long-period phenotype of *Cry2*-knockout mice and the short-period phenotype of knockdown of *Dyrk1a* in cultured cells with abnormal accumulation of CRY2 protein (Kurabayashi et al., 2010; Thresher et al., 1998). It could not have ruled out the possibility that short-period phenotype of the *Adar2*-knockout mice are associated with alteration of the master clock oscillation in the SCN neuronal network, since A-to-I RNA editing have an critical role of neuronal activities in CNS. Recent study revealed that *Adar2*-mediated RNA editing of the Ca_V 1.3 IQ-domain modulates potential firing rates of SCN slice, although they did not mention the effect on daily variation of SCN firing rates (Huang et al., 2012a). In addition, rhythmic locomotor activity experiments in *Drosophila* under light-dark (12:12 hr) condition on hypomorphic allele of *drosophila Adar* gene, which is homologous to the mammalian RNA editing enzyme ADAR2, showed the decreased anticipation of dark-light transitions with reduced locomotor activity (Jepson et al., 2011). The experiment suggested the importance of *dAdar* on circadian oscillation, though they could not rule out the possibility that either light or decreasing locomotor activity affected the decreased anticipation phenotype. However, I emphasize that the short-period rhythms of gene expression profiles in transcriptome data reliably demonstrates the physiological importance of *Adar2* on circadian oscillations in every tissues in the body.

A statistically significant about 15-min decrease in circadian period of *Adar2*$^{-/-}$ / *Gria2*$^{R/R}$ mice is similar magnitude to that observed in single knockout of circadian clock components (Fig. 25). On the other hand, mammalian circadian clock are often regulated by several redundant mechanisms. For example, double-knockout mice for CLOCK/NPAS2, CRY1/CRY2 and PER1/PER2 exhibit complete loss of circadian rhythmicity in wheel-running activity and gene expression (Bae et al., 2001; DeBruyne

et al., 2007; van der Horst et al., 1999; Vitaterna et al., 1999; Zheng et al., 2001). In mammals, *Adar1* and *Adar2* coordinately mediate A-to-I RNA editing suggesting the possibility that double-knockout of *Adar1* and *Adar2* might show severe phenotype for rhythmicity. Further study is needed.

There had been very few reports referring the relationship of circadian rhythm and RNA editing. The Nitabach laboratory demonstrated that A-to-I RNA editing did not show any evidence of circadian oscillation in fly heads (Hughes et al., 2012), probably due to tissue limitation. According to my results, only faint editing rhythms were found in several regions of murine brain (data not shown). Hence A-to-I RNA editing were known to be tissue-specifically regulated, I speculate that fly head or mouse brain exhibited no editing rhythms as a result of cell heterogeneity, whereas liver largely consists of hepatocytes. Instead, Nitabach and colleagues revealed that functional loss of *period* significantly altered the levels of RNA editing at several editing sites. My study suggests the possibility that *period* loss alters expression levels of *Clock* and the downstream *Adar* expression levels resulting in the global changes of editing levels.

Collectively, I elucidated the circadian expression of *Adar2* by CLOCK-dependent transactivation, and illustrated the rhythmic profiles of *Adar2*-dependent editing events in a genome-wide manner. In addition, I demonstrated the significant mechanism that *Adar2* plays an essential role for the robust circadian oscillation by suppressing CRY2 expression through the regulation of miRNA biogenesis. Furthermore, I emphasized that *Adar2*-mediated post-transcriptional regulation significantly contributed to circadian profiles of steady-state mRNA levels and global circadian outputs (Fig. 33).

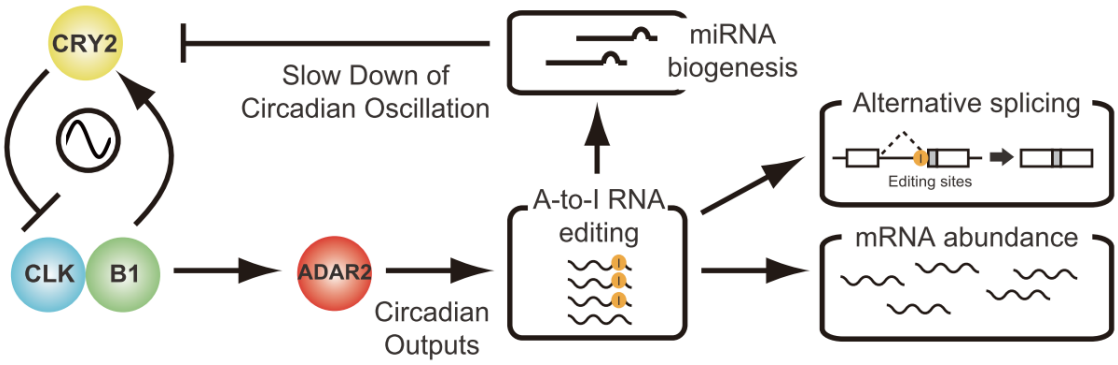

Figure 33 Models for the *Adar2*-mediated regulations of the rhythmical RNA editing events and global circadian outputs

See text for details.

4 Conclusions

In the first part of this study, I demonstrated CLOCK-controlled rhythmic regulation of KLF transcription factors, lncRNAs and miRNAs. Rhythmically expressed miRNAs lead to circadian expression profiles of their target mRNAs. In addition, alternative splicing events are also regulated in a circadian manner. These results indicate important contributions of indirect regulations and post-transcriptional regulations on dynamic circadian outputs. In particular, I established the functional crosstalk between circadian rhythm and A-to-I RNA editing for the first time, in the second part of this study. A-to-I RNA editing enzyme *Adar2* is rhythmically transcribed by CLOCK-BMAL1 complex in mouse liver. As a result, *Adar2*-mediated A-to-I RNA modification in mRNAs and *Adar2*-dependent alternative splicing exhibit circadian profiles. The RNA-Seq analysis identified various rhythmic editing sites, which are largely dependent on *Adar2*, and their peak phases show significant enrichment during dusk phase. Furthermore, a large number of transcripts oscillations are attenuated in *Adar2*-knockout mice, suggesting that cyclic profiles of various RNA accumulation are post-transcriptionally produced by *Adar2*. On the other hand, *Adar2* inhibits expression of CRY2 proteins through a regulation of miRNA let-7g biogenesis, which has a pivotal function in circadian period of gene expression and locomotor activity.

Collectively, a rhythmic post-transcriptional regulation of A-to-I RNA editing plays an essential role in generating global circadian outputs, in addition, circadian clock itself needs to A-to-I RNA editing for normal circadian rhythmicity.

5 References

Asher, G., and Schibler, U. (2011). Crosstalk between components of circadian and metabolic cycles in mammals. Cell Metab. *13*, 125–137.

Bae, K., Jin, X., Maywood, E.S., Hastings, M.H., Reppert, S.M., and Weaver, D.R. (2001). Differential functions of mPer1, mPer2, and mPer3 in the SCN circadian clock. Neuron *30*, 525–536.

Barbon, A., Vallini, I., La Via, L., Marchina, E., and Barlati, S. (2003). Glutamate receptor RNA editing: a molecular analysis of GluR2, GluR5 and GluR6 in human brain tissues and in NT2 cells following in vitro neural differentiation. Brain Res. Mol. Brain Res. *117*, 168–178.

Barnett, D.W., Garrison, E.K., Quinlan, A.R., Strömberg, M.P., and Marth, G.T. (2011). BamTools: a C++ API and toolkit for analyzing and managing BAM files. Bioinforma. Oxf. Engl. *27*, 1691–1692.

Bertram, L., Hiltunen, M., Parkinson, M., Ingelsson, M., Lange, C., Ramasamy, K., Mullin, K., Menon, R., Sampson, A.J., Hsiao, M.Y., et al. (2005). Family-based association between Alzheimer's disease and variants in UBQLN1. N. Engl. J. Med. *352*, 884–894.

Betel, D., Wilson, M., Gabow, A., Marks, D.S., and Sander, C. (2008). The microRNA.org resource: targets and expression. Nucleic Acids Res. *36*, D149–D153.

Chan, P.P., and Lowe, T.M. (2009). GtRNAdb: a database of transfer RNA genes detected in genomic sequence. Nucleic Acids Res. *37*, D93–D97.

Chen, C.X., Cho, D.S., Wang, Q., Lai, F., Carter, K.C., and Nishikura, K. (2000). A third member of the RNA-specific adenosine deaminase gene family, ADAR3, contains both single- and double-stranded RNA binding domains. RNA N. Y. N *6*, 755–767.

Chen, R., D'Alessandro, M., and Lee, C. (2013). miRNAs are required for generating a time delay critical for the circadian oscillator. Curr. Biol. CB *23*, 1959–1968.

Cheng, H.-Y.M., Papp, J.W., Varlamova, O., Dziema, H., Russell, B., Curfman, J.P.,

Nakazawa, T., Shimizu, K., Okamura, H., Impey, S., et al. (2007). microRNA modulation of circadian-clock period and entrainment. Neuron *54*, 813–829.

DeBruyne, J.P., Weaver, D.R., and Reppert, S.M. (2007). CLOCK and NPAS2 have overlapping roles in the suprachiasmatic circadian clock. Nat. Neurosci. *10*, 543–545.

Du, N.-H., Arpat, A.B., De Matos, M., and Gatfield, D. (2014). MicroRNAs shape circadian hepatic gene expression on a transcriptome-wide scale. eLife *3*, e02510.

Dunlap, J.C. (1999). Molecular bases for circadian clocks. Cell *96*, 271–290.

Duong, H.A., Robles, M.S., Knutti, D., and Weitz, C.J. (2011). A molecular mechanism for circadian clock negative feedback. Science *332*, 1436–1439.

Fustin, J.-M., Doi, M., Yamaguchi, Y., Hida, H., Nishimura, S., Yoshida, M., Isagawa, T., Morioka, M.S., Kakeya, H., Manabe, I., et al. (2013). RNA-Methylation-Dependent RNA Processing Controls the Speed of the Circadian Clock. Cell *155*, 793–806.

Gallego, M., and Virshup, D.M. (2007). Post-translational modifications regulate the ticking of the circadian clock. Nat. Rev. Mol. Cell Biol. *8*, 139–148.

Garcia, D.M., Baek, D., Shin, C., Bell, G.W., Grimson, A., and Bartel, D.P. (2011). Weak seed-pairing stability and high target-site abundance decrease the proficiency of lsy-6 and other microRNAs. Nat. Struct. Mol. Biol. *18*, 1139–1146.

Gatfield, D., Le Martelot, G., Vejnar, C.E., Gerlach, D., Schaad, O., Fleury-Olela, F., Ruskeepää, A.-L., Oresic, M., Esau, C.C., Zdobnov, E.M., et al. (2009). Integration of microRNA miR-122 in hepatic circadian gene expression. Genes Dev. *23*, 1313–1326.

Haapasalo, A., Viswanathan, J., Kurkinen, K.M., Bertram, L., Soininen, H., Dantuma, N.P., Tanzi, R.E., and Hiltunen, M. (2011). Involvement of ubiquilin-1 transcript variants in protein degradation and accumulation. Commun. Integr. Biol. *4*, 428–432.

Hartner, J.C., Schmittwolf, C., Kispert, A., Müller, A.M., Higuchi, M., and Seeburg, P.H. (2004). Liver disintegration in the mouse embryo caused by deficiency in the RNA-editing enzyme ADAR1. J. Biol. Chem. *279*, 4894–4902.

Hastings, M.H., Reddy, A.B., and Maywood, E.S. (2003). A clockwork web: circadian timing in brain and periphery, in health and disease. Nat. Rev. Neurosci. *4*, 649–661.

Hatori, M., Gill, S., Mure, L.S., Goulding, M., O'Leary, D.D., and Panda, S. (2014). Lhx1 maintains synchrony among circadian oscillator neurons of the SCN. eLife e03357.

Higuchi, M., Maas, S., Single, F.N., Hartner, J., Rozov, A., Burnashev, N., Feldmeyer, D., Sprengel, R., and Seeburg, P.H. (2000). Point mutation in an AMPA receptor gene rescues lethality in mice deficient in the RNA-editing enzyme ADAR2. Nature *406*, 78–81.

Hirano, A., Yumimoto, K., Tsunematsu, R., Matsumoto, M., Oyama, M., Kozuka-Hata, H., Nakagawa, T., Lanjakornsiripan, D., Nakayama, K.I., and Fukada, Y. (2013). FBXL21 regulates oscillation of the circadian clock through ubiquitination and stabilization of cryptochromes. Cell *152*, 1106–1118.

Hirota, T., Kon, N., Itagaki, T., Hoshina, N., Okano, T., and Fukada, Y. (2010). Transcriptional repressor TIEG1 regulates Bmal1 gene through GC box and controls circadian clockwork. Genes Cells Devoted Mol. Cell. Mech. *15*, 111–121.

Hogg, M., Paro, S., Keegan, L.P., and O'Connell, M.A. (2011). RNA editing by mammalian ADARs. Adv. Genet. *73*, 87–120.

Van der Horst, G.T., Muijtjens, M., Kobayashi, K., Takano, R., Kanno, S., Takao, M., de Wit, J., Verkerk, A., Eker, A.P., van Leenen, D., et al. (1999). Mammalian Cry1 and Cry2 are essential for maintenance of circadian rhythms. Nature *398*, 627–630.

Hu, Y., Leo, C., Yu, S., Huang, B.C.B., Wang, H., Shen, M., Luo, Y., Daniel-Issakani, S., Payan, D.G., and Xu, X. (2004). Identification and functional characterization of a novel human misshapen/Nck interacting kinase-related kinase, hMINK beta. J. Biol. Chem. *279*, 54387–54397.

Huang, H., Tan, B.Z., Shen, Y., Tao, J., Jiang, F., Sung, Y.Y., Ng, C.K., Raida, M., Köhr, G., Higuchi, M., et al. (2012a). RNA editing of the IQ domain in Ca(v)1.3 channels modulates their Ca^{2+}-dependent inactivation. Neuron *73*, 304–316.

Huang, N., Chelliah, Y., Shan, Y., Taylor, C.A., Yoo, S.-H., Partch, C., Green, C.B., Zhang,

H., and Takahashi, J.S. (2012b). Crystal structure of the heterodimeric CLOCK:BMAL1 transcriptional activator complex. Science *337*, 189–194.

Hughes, M.E., Hogenesch, J.B., and Kornacker, K. (2010). JTK_CYCLE: an efficient nonparametric algorithm for detecting rhythmic components in genome-scale data sets. J. Biol. Rhythms *25*, 372–380.

Hughes, M.E., Grant, G.R., Paquin, C., Qian, J., and Nitabach, M.N. (2012). Deep sequencing the circadian and diurnal transcriptome of Drosophila brain. Genome Res.

Jagannath, A., Butler, R., Godinho, S.I.H., Couch, Y., Brown, L.A., Vasudevan, S.R., Flanagan, K.C., Anthony, D., Churchill, G.C., Wood, M.J.A., et al. (2013). The CRTC1-SIK1 Pathway Regulates Entrainment of the Circadian Clock. Cell *154*, 1100–1111.

Jepson, J.E.C., Savva, Y.A., Yokose, C., Sugden, A.U., Sahin, A., and Reenan, R.A. (2011). Engineered alterations in RNA editing modulate complex behavior in Drosophila: regulatory diversity of adenosine deaminase acting on RNA (ADAR) targets. J. Biol. Chem. *286*, 8325–8337.

Jeyaraj, D., Haldar, S.M., Wan, X., McCauley, M.D., Ripperger, J.A., Hu, K., Lu, Y., Eapen, B.L., Sharma, N., Ficker, E., et al. (2012a). Circadian rhythms govern cardiac repolarization and arrhythmogenesis. Nature *483*, 96–99.

Jeyaraj, D., Scheer, F.A.J.L., Ripperger, J.A., Haldar, S.M., Lu, Y., Prosdocimo, D.A., Eapen, S.J., Eapen, B.L., Cui, Y., Mahabeleshwar, G.H., et al. (2012b). Klf15 orchestrates circadian nitrogen homeostasis. Cell Metab. *15*, 311–323.

Jouffe, C., Cretenet, G., Symul, L., Martin, E., Atger, F., Naef, F., and Gachon, F. (2013). The circadian clock coordinates ribosome biogenesis. PLoS Biol. *11*, e1001455.

Kawahara, Y., Zinshteyn, B., Chendrimada, T.P., Shiekhattar, R., and Nishikura, K. (2007a). RNA editing of the microRNA-151 precursor blocks cleavage by the Dicer-TRBP complex. EMBO Rep. *8*, 763–769.

Kawahara, Y., Zinshteyn, B., Sethupathy, P., Iizasa, H., Hatzigeorgiou, A.G., and Nishikura, K. (2007b). Redirection of silencing targets by adenosine-to-inosine editing of

miRNAs. Science *315*, 1137–1140.

Kawahara, Y., Megraw, M., Kreider, E., Iizasa, H., Valente, L., Hatzigeorgiou, A.G., and Nishikura, K. (2008). Frequency and fate of microRNA editing in human brain. Nucleic Acids Res. *36*, 5270–5280.

Kim, D., Pertea, G., Trapnell, C., Pimentel, H., Kelley, R., and Salzberg, S.L. (2013). TopHat2: accurate alignment of transcriptomes in the presence of insertions, deletions and gene fusions. Genome Biol. *14*, R36.

Kim, D.-Y., Woo, K.-C., Lee, K.-H., Kim, T.-D., and Kim, K.-T. (2010). hnRNP Q and PTB modulate the circadian oscillation of mouse Rev-erb alpha via IRES-mediated translation. Nucleic Acids Res. *38*, 7068–7078.

Kiran, A.M., O'Mahony, J.J., Sanjeev, K., and Baranov, P.V. (2012). Darned in 2013: inclusion of model organisms and linking with Wikipedia. Nucleic Acids Res. *41*, D258–D261.

Koike, N., Yoo, S.-H., Huang, H.-C., Kumar, V., Lee, C., Kim, T.-K., and Takahashi, J.S. (2012). Transcriptional Architecture and Chromatin Landscape of the Core Circadian Clock in Mammals. Science *338*, 349–354.

Kojima, S., Shingle, D.L., and Green, C.B. (2011). Post-transcriptional control of circadian rhythms. J. Cell Sci. *124*, 311–320.

Kojima, S., Sher-Chen, E.L., and Green, C.B. (2012). Circadian control of mRNA polyadenylation dynamics regulates rhythmic protein expression. Genes Dev. *26*, 2724–2736.

Kon, N., Hirota, T., Kawamoto, T., Kato, Y., Tsubota, T., and Fukada, Y. (2008). Activation of TGF-beta/activin signalling resets the circadian clock through rapid induction of Dec1 transcripts. Nat. Cell Biol. *10*, 1463–1469.

Kon, N., Yoshikawa, T., Honma, S., Yamagata, Y., Yoshitane, H., Shimizu, K., Sugiyama, Y., Hara, C., Kameshita, I., Honma, K., et al. (2014). CaMKII is essential for the cellular clock and coupling between morning and evening behavioral rhythms. Genes Dev. *28*,

1101–1110.

Kondratov, R.V., Kondratova, A.A., Lee, C., Gorbacheva, V.Y., Chernov, M.V., and Antoch, M.P. (2006). Post-translational regulation of circadian transcriptional CLOCK(NPAS2)/BMAL1 complex by CRYPTOCHROMES. Cell Cycle Georget. Tex *5*, 890–895.

Kurabayashi, N., Hirota, T., Sakai, M., Sanada, K., and Fukada, Y. (2010). DYRK1A and glycogen synthase kinase 3beta, a dual-kinase mechanism directing proteasomal degradation of CRY2 for circadian timekeeping. Mol. Cell. Biol. *30*, 1757–1768.

Lee, C., Etchegaray, J.P., Cagampang, F.R., Loudon, A.S., and Reppert, S.M. (2001). Posttranslational mechanisms regulate the mammalian circadian clock. Cell *107*, 855–867.

Lee, K.-H., Kim, S.-H., Kim, H.-J., Kim, W., Lee, H.-R., Jung, Y., Choi, J.-H., Hong, K.Y., Jang, S.K., and Kim, K.-T. (2014). AUF1 contributes to Cryptochrome1 mRNA degradation and rhythmic translation. Nucleic Acids Res. *42*, 3590–3606.

Lim, C., and Allada, R. (2013). Emerging roles for post-transcriptional regulation in circadian clocks. Nat. Neurosci. *16*, 1544–1550.

Lin, D.-H., Yue, P., Pan, C., Sun, P., and Wang, W.-H. (2011). MicroRNA 802 stimulates ROMK channels by suppressing caveolin-1. J. Am. Soc. Nephrol. JASN *22*, 1087–1098.

Maas, S., Patt, S., Schrey, M., and Rich, A. (2001). Underediting of glutamate receptor GluR-B mRNA in malignant gliomas. Proc. Natl. Acad. Sci. U. S. A. *98*, 14687–14692.

Mallela, A., and Nishikura, K. (2012). A-to-I editing of protein coding and noncoding RNAs. Crit. Rev. Biochem. Mol. Biol.

Le Martelot, G., Canella, D., Symul, L., Migliavacca, E., Gilardi, F., Liechti, R., Martin, O., Harshman, K., Delorenzi, M., Desvergne, B., et al. (2012). Genome-Wide RNA Polymerase II Profiles and RNA Accumulation Reveal Kinetics of Transcription and Associated Epigenetic Changes During Diurnal Cycles. PLoS Biol. *10*, e1001442.

Martin, M. (2011). Cutadapt removes adapter sequences from high-throughput

sequencing reads. EMBnet.journal *17*, pp. 10–12.

McConnell, B.B., and Yang, V.W. (2010). Mammalian Krüppel-like factors in health and diseases. Physiol. Rev. *90*, 1337–1381.

McGlincy, N.J., Valomon, A., Chesham, J.E., Maywood, E.S., Hastings, M.H., and Ule, J. (2012). Regulation of alternative splicing by the circadian clock and food related cues. Genome Biol. *13*, R54.

Menet, J.S., Rodriguez, J., Abruzzi, K.C., and Rosbash, M. (2012). Nascent-Seq reveals novel features of mouse circadian transcriptional regulation. eLife *1*, e00011.

Mohawk, J.A., Green, C.B., and Takahashi, J.S. (2012). Central and Peripheral Circadian Clocks in Mammals. Annu. Rev. Neurosci.

Nishikura, K. (2010). Functions and regulation of RNA editing by ADAR deaminases. Annu. Rev. Biochem. *79*, 321–349.

Oster, H., Damerow, S., Hut, R.A., and Eichele, G. (2006). Transcriptional profiling in the adrenal gland reveals circadian regulation of hormone biosynthesis genes and nucleosome assembly genes. J. Biol. Rhythms *21*, 350–361.

Plath, K., Mlynarczyk-Evans, S., Nusinow, D.A., and Panning, B. (2002). Xist RNA and the mechanism of X chromosome inactivation. Annu. Rev. Genet. *36*, 233–278.

Preußner, M., Wilhelmi, I., Schultz, A.-S., Finkernagel, F., Michel, M., Möröy, T., and Heyd, F. (2014). Rhythmic U2af26 Alternative Splicing Controls PERIOD1 Stability and the Circadian Clock in Mice. Mol. Cell.

Ramaswami, G., and Li, J.B. (2014). RADAR: a rigorously annotated database of A-to-I RNA editing. Nucleic Acids Res. *42*, D109–D113.

Reppert, S.M., and Weaver, D.R. (2002). Coordination of circadian timing in mammals. Nature *418*, 935–941.

Ripperger, J.A., and Schibler, U. (2006). Rhythmic CLOCK-BMAL1 binding to multiple E-box motifs drives circadian Dbp transcription and chromatin transitions. Nat. Genet.

38, 369–374.

Rueter, S.M., Dawson, T.R., and Emeson, R.B. (1999). Regulation of alternative splicing by RNA editing. Nature *399*, 75–80.

Sakurai, M., Ueda, H., Yano, T., Okada, S., Terajima, H., Mitsuyama, T., Toyoda, A., Fujiyama, A., Kawabata, H., and Suzuki, T. (2014). A biochemical landscape of A-to-I RNA editing in the human brain transcriptome. Genome Res. *24*, 522–534.

Sasaki, M., Yoshitane, H., Du, N.-H., Okano, T., and Fukada, Y. (2009). Preferential inhibition of BMAL2-CLOCK activity by PER2 reemphasizes its negative role and a positive role of BMAL2 in the circadian transcription. J. Biol. Chem. *284*, 25149–25159.

Scadden, A.D.J. (2005). The RISC subunit Tudor-SN binds to hyper-edited double-stranded RNA and promotes its cleavage. Nat. Struct. Mol. Biol. *12*, 489–496.

Shimba, S., Ogawa, T., Hitosugi, S., Ichihashi, Y., Nakadaira, Y., Kobayashi, M., Tezuka, M., Kosuge, Y., Ishige, K., Ito, Y., et al. (2011). Deficient of a Clock Gene, Brain and Muscle Arnt-Like Protein-1 (BMAL1), Induces Dyslipidemia and Ectopic Fat Formation. PloS One *6*, e25231.

Spörl, F., Korge, S., Jürchott, K., Wunderskirchner, M., Schellenberg, K., Heins, S., Specht, A., Stoll, C., Klemz, R., Maier, B., et al. (2012). Kruppel-like factor 9 is a circadian transcription factor in human epidermis that controls proliferation of keratinocytes. Proc. Natl. Acad. Sci. U. S. A. *109*, 10903–10908.

St Laurent, G., Tackett, M.R., Nechkin, S., Shtokalo, D., Antonets, D., Savva, Y.A., Maloney, R., Kapranov, P., Lawrence, C.E., and Reenan, R.A. (2013). Genome-wide analysis of A-to-I RNA editing by single-molecule sequencing in Drosophila. Nat. Struct. Mol. Biol. *20*, 1333–1339.

Svingen, T., Spiller, C.M., Kashimada, K., Harley, V.R., and Koopman, P. (2009). Identification of suitable normalizing genes for quantitative real-time RT-PCR analysis of gene expression in fetal mouse gonads. Sex. Dev. Genet. Mol. Biol. Evol. Endocrinol. Embryol. Pathol. Sex Determ. Differ. *3*, 194–204.

Thresher, R.J., Vitaterna, M.H., Miyamoto, Y., Kazantsev, A., Hsu, D.S., Petit, C., Selby, C.P., Dawut, L., Smithies, O., Takahashi, J.S., et al. (1998). Role of mouse cryptochrome blue-light photoreceptor in circadian photoresponses. Science *282*, 1490–1494.

Trapnell, C., Williams, B.A., Pertea, G., Mortazavi, A., Kwan, G., van Baren, M.J., Salzberg, S.L., Wold, B.J., and Pachter, L. (2010). Transcript assembly and quantification by RNA-Seq reveals unannotated transcripts and isoform switching during cell differentiation. Nat. Biotechnol. *28*, 511–515.

Vesely, C., Tauber, S., Sedlazeck, F.J., von Haeseler, A., and Jantsch, M.F. (2012). Adenosine deaminases that act on RNA induce reproducible changes in abundance and sequence of embryonic miRNAs. Genome Res. *22*, 1468–1476.

Vitaterna, M.H., Selby, C.P., Todo, T., Niwa, H., Thompson, C., Fruechte, E.M., Hitomi, K., Thresher, R.J., Ishikawa, T., Miyazaki, J., et al. (1999). Differential regulation of mammalian period genes and circadian rhythmicity by cryptochromes 1 and 2. Proc. Natl. Acad. Sci. U. S. A. *96*, 12114–12119.

Vollmers, C., Schmitz, R.J., Nathanson, J., Yeo, G., Ecker, J.R., and Panda, S. (2012). Circadian Oscillations of Protein-Coding and Regulatory RNAs in a Highly Dynamic Mammalian Liver Epigenome. Cell Metab. *16*, 833–845.

Wang, K., Singh, D., Zeng, Z., Coleman, S.J., Huang, Y., Savich, G.L., He, X., Mieczkowski, P., Grimm, S.A., Perou, C.M., et al. (2010). MapSplice: accurate mapping of RNA-seq reads for splice junction discovery. Nucleic Acids Res. *38*, e178.

Westergaard, G.G., Bercovich, N., Reinert, M.D., and Vazquez, M.P. (2010). Analysis of a nuclear localization signal in the p14 splicing factor in Trypanosoma cruzi. Int. J. Parasitol. *40*, 1029–1035.

Woo, K.-C., Kim, T.-D., Lee, K.-H., Kim, D.-Y., Kim, W., Lee, K.-Y., and Kim, K.-T. (2009). Mouse period 2 mRNA circadian oscillation is modulated by PTB-mediated rhythmic mRNA degradation. Nucleic Acids Res. *37*, 26–37.

Woo, K.-C., Ha, D.-C., Lee, K.-H., Kim, D.-Y., Kim, T.-D., and Kim, K.-T. (2010). Circadian amplitude of cryptochrome 1 is modulated by mRNA stability regulation via cytoplasmic

hnRNP D oscillation. Mol. Cell. Biol. *30*, 197–205.

Wulff, B.-E., Sakurai, M., and Nishikura, K. (2011). Elucidating the inosinome: global approaches to adenosine-to-inosine RNA editing. Nat. Rev. Genet. *12*, 81–85.

Yang, R., and Su, Z. (2010). Analyzing circadian expression data by harmonic regression based on autoregressive spectral estimation. Bioinforma. Oxf. Engl. *26*, i168–i174.

Yoshitane, H., Takao, T., Satomi, Y., Du, N.-H., Okano, T., and Fukada, Y. (2009). Roles of CLOCK phosphorylation in suppression of E-box-dependent transcription. Mol. Cell. Biol. *29*, 3675–3686.

Yoshitane, H., Honma, S., Imamura, K., Nakajima, H., Nishide, S.-Y., Ono, D., Kiyota, H., Shinozaki, N., Matsuki, H., Wada, N., et al. (2012). JNK regulates the photic response of the mammalian circadian clock. EMBO Rep.

Yoshitane, H., Ozaki, H., Terajima, H., Du, N.-H., Suzuki, Y., Fujimori, T., Kosaka, N., Shimba, S., Sugano, S., Takagi, T., et al. (2014). CLOCK-controlled polyphonic regulation of circadian rhythms through canonical and noncanonical E-boxes. Mol. Cell. Biol. *34*, 1776–1787.

Zheng, B., Albrecht, U., Kaasik, K., Sage, M., Lu, W., Vaishnav, S., Li, Q., Sun, Z.S., Eichele, G., Bradley, A., et al. (2001). Nonredundant roles of the mPer1 and mPer2 genes in the mammalian circadian clock. Cell *105*, 683–694.

6 Acknowledgements

First of all, I would like to show my greatest appreciation to my supervisor, Professor Yoshitaka Fukada, for his constructive discussion and enormous encouragement throughout my study. I am deeply grateful to Dr. Hikari Yoshitane for his helpful comments and advice for experimental techniques. I would also like to express my gratitude to Dr. Wataru Iwasaki for his insightful advice and suggestions. I thank Haruka Ozaki and Tomoki Nakagawa for their help with RNA-Seq data analyses. I am also grateful to Dr. Yutaka Suzuki, Ngoc-Hien Du, Taihei Fujimori and Naoki Kosaka for their experimental assistance. I received generous support from Dr. Daisuke Kojima, Dr. Kimiko Shimizu, Dr. Masaki Torii, Dr. Tomoya Shiraki and the other members of Fukada laboratory for meaningful discussion and joyful days. This study was achieved by collaborations with Dr. Shigeki Shimba for Bmal1-knockout mice. *Adar2*$^{-/-}$ / *Gria2*$^{R/R}$ mice were obtained from the Mutant Mouse Regional Resource Center (MMRRC) 8U42OD010924-13. I would like to thank Japan Society for Promotion of Science (JSPS) Research Fellowships for Young Scientists for financial support during my graduate study. The super-computing resource was provided by Human Genome Center (The Univ. of Tokyo). Finally, I would like to offer my special thanks to my parents for their warm encouragement and financial support. Without their constant support, this paper would not have been possible.

7 List of Publications

Yoshitane Hikari*, Haruka Ozaki*, Hideki Terajima*, Ngoc-Hien Du, Yutaka Suzuki, Taihei Fujimori, Naoki Kosaka, Shigeki Shimba, Sumio Sugano, Toshihisa Takagi, Wataru Iwasaki, Yoshitaka Fukada

CLOCK-Controlled Polyphonic Regulations of Circadian Rhythms through Canonical and Non-Canonical E-Boxes. *Molecular and Cellular Biology*, **34 (10)**, 1776-1787 (2014)

* These authors contributed equally to this work.

Table 1　Primers for cloning, qRT-PCR and sequencing

primer_name	primer sequences (5' → 3')
mir-802 cloning Fw	CGGGATCCGCAGAGACGGAAGAGGATAC
mir-802 cloning Rv	CCGCTCGAGTTACTATGTCAGAAGGCAGCG
Cav1-3'UTR cloning Fw	GCCGTGTAATTCTAGTCAAGGATGAAAGGTTTTTTTCCC
Cav1-3'UTR cloning Rv	CCGCCCCGACTCTAGTTATAGGACATGCAGCATAAAAAAGTG
Cry2-3'UTR cloning Fw	GACTGGAGAGCCATCGCTCC
Cry2-3'UTR cloning Rv	TTTTACTCAGACAGGATCAG
Tbp-Fw	ATGGTGTGCACAGGAGCCAAG
Tbp-Rv	TCATAGCTACTGAACTGCTG
Klf11-Fw	AAGCTCATCTTCGCACTCAC
Klf11-Rv	AACTTCTTGTCACAGCCGTC
Klf13-Rv	GGGAAATCTTCGCACCTC
Klf13-Rv	ATAGTGCCGTGCCAGCTC
pri-mir-802-Fw	GATGAGAGGACGCTGTTCGC
pri-mir-802-Rv	CGCTTATCCACGAGAAACGC
0610005C13Rik-Fw	TCCATCTATGACACCGCTTG
0610005C13Rik-Rv	GCGTTTACTGTTGTGCGTTC
Ubqln1-Fw	CAGTCCCTGAGCCAGAAC
Ubqln1-inRv	ATTATTCAGCATCATCTGCG
Ubqln1-exRv	GGGTTCTGCATCTGCG
Mink1-Fw	GCCAAGCCTGAAGACCAC
Mink1-inRv	AATTGCTCGCTTATAGCTTGC
Mink1-exRv	TTTGAGCAACACAAAGTCTGC
Rps29-Fw	TGAAGGCAAGATGGGTCAC
Rps29-Rv	GCACATGTTCAGCCCGTATT
Adar2-Fw	TTGCCCTGAAGGAGTTTTG
Adar2-Rv	GAGGGCTTCTTGACTGGC
Adar1 p150-Fw	TCTCAAGGGTTCAGGGGAC
Adar1 p150-Rv	TACGACTGTGTCTGGTGAGGG
Adar1 p110-Fw	TTGGGACTAGCCGGGAAG
Adar1 p110-Rv	TACGACTGTGTCTGGTGAGGG
Adar2 long-Fw	AAAAGAGGTCTCCGCCAGTC
Adar2 long-Rv	TGTGGTGCCCAGAAAGAGTAAC
Dbp-Fw	AATGACCTTTGAACCTGATCCCGCT
Dbp-Rv	GCTCCAGTACTTCTCATCCTTCTGT
Per1-Fw	CAGGCTAACCAGGAATATTACCAGC
Per1-Rv	CACAGCCACAGAGAAGGTGTCCTGG
Per2-Fw	GGCTTCACCATGCCTGTTGT
Per2-Rv	GGAGTTATTTCGGAGGCAAGTGT
Cry1-Fw	CCCAGGCTTTTCAAGGAATGGAACA
Cry1-Rv	TCTCATCATGGTCATCAGACAGAGG
Cry2-Fw	GGGACTCTGTCTATTGGCATCTG
Cry2-Rv	GTCACTCTAGCCCGCTTGGT

Clock-Fw	CCTATCCTACCTTGGCCACACA
Clock-Rv	TCCCGTGGAGCAACCTAGAT
Npas2-Fw	ATGCTGCCGTCTGTTGTC
Npas2-Rv	AAGAATTCACCCAGCTGATG
Bmal1-Fw	GCAGTGCCACTGACTACCAAGA
Bmal1-Rv	TCCTGGACATTGCATTGCAT
Reverbα-Fw	CGTTCGCATCAATCGCAACC
Reverbα-Rv	GATGTGGAGTAGGTGAGGTC
Reverbβ-Fw	ACGGATTCCCAGGAACATGG
Reverbβ-Rv	CCTCCAGTGTTGCACAGGTA
Dec1-Fw	ATCAGCCTCCTTTTTGCCTTC
Dec1-Rv	AGCATTTCTCCAGCATAGGCAG
Dec2-Fw	ATTGCTTTACAGAATGGGGAGCG
Dec2-Rv	AAAGCGCGCGAGGTATTGCAAGAC
Slco1a4-Fw	GGGAAAATCTGAGAAAGAGG
Slco1a4-Rv	GTTAATGCCAACAGAAATGC
Aim1l-Fw	TCTCCAAGGCTTTGGCTC
Aim1l-Rv	AGGCTGATCCTGGGAGTG
Ugt2b38-Fw	AAGAAATGGGACTCATTTTACAG
Ugt2b38-Rv	TTGTCTCAGCTAAGGTGGTG
pri-let-7g-Fw	GTGCACCAGCTACCAAATG
pri-let-7g-Rv	AATCCCAGAGATGAGCAGG
Flnb-seqFw1	CCCAGCTGAGTTCAGCATCTGGAC
Flnb-seqRv1	CTTGACATCGATCGTGTGGATGC
Flnb-seqFw2	CGGCCTCTCCATTGCTGTTG
Flnb-seqRv2	ATTCTCATGCGGGATGAAGCG
Cog3-seqFw1	CCAAGGATTATCACAGGAAGC
Cog3-seqRv1	GCCTAAAAAATCGTGGAACAG
Cog3-seqFw2	GCCTTGTCTGCCTGCATAC
Cog3-seqRv2	AAAAAATCGTGGAACAGTCATAG
Copa-seqFw1	TGAGCGCCTCAGATGATCAGAC
Copa-seqRv1	CAACCTCCCATGCCTTTGATTC
Copa-seqFw2	TCAGATGATCAGACCATTCGGG
Copa-seqRv2	TGCCTTTGATTCATTCATACGCC
Cdk13-seqFw1	CCTCTGCTCTTCCTGGCTG
Cdk13-seqRv1	CGGACTGGGAGCTCACATC
Cdk13-seqFw2	CTCTGCTCTTCCTGGCTGC
Cdk13-seqRv2	ACTGGGAGCTCACATCCTCG
Azin1-seqFw1	GAGTGATGAGCCAGCCTTC
Azin1-seqRv1	CCAGCATCTTGCATCTCATAC
Azin1-seqFw2	GATGAGCCAGCCTTCGTG
Azin1-seqRv2	GCATCTTGCATCTCATACCAATC
Rpa1-seqFw1	ATCAAAGGCCTATCGTTAATATC
Rpa1-seqRv1	CTGATGCAAACTGAAGCC
Rpa1-seqFw2	CAAAGGCCTATCGTTAATATCTG
Rpa1-seqRv2	CTGTAGCAGCCTGGATGTC

Table 2 Number of sequenced tags of RNA-Seq

RNA samples	total tags	unmapped tags	(%)	mapped tags					
				all	(%)	unique	(%)	multi	(%)
WT CT02-1	91,801,028	1,684,628	1.8	90,116,400	98.2	89,344,882	97.3	771,518	0.8
WT CT02-2	51,193,078	2,103,921	4.1	49,089,157	95.9	48,628,433	95.0	460,724	0.9
WT CT06-1	72,257,200	3,121,691	4.3	69,135,509	95.7	68,611,427	95.0	524,082	0.7
WT CT06-2	76,755,656	4,979,295	6.5	71,776,361	93.5	71,120,925	92.7	655,436	0.9
WT CT10-1	59,571,486	3,098,682	5.2	56,472,804	94.8	55,990,862	94.0	481,942	0.8
WT CT10-2	53,959,212	1,860,685	3.4	52,098,527	96.6	51,645,281	95.7	453,246	0.8
WT CT14-1	65,175,622	3,444,904	5.3	61,730,718	94.7	61,161,570	93.8	569,148	0.9
WT CT14-2	49,127,454	2,669,186	5.4	46,458,268	94.6	45,931,142	93.5	527,126	1.1
WT CT18-1	76,180,484	3,610,642	4.7	72,569,842	95.3	71,969,026	94.5	600,816	0.8
WT CT18-2	58,597,338	3,653,461	6.2	54,943,877	93.8	54,472,373	93.0	471,504	0.8
WT CT22-1	81,568,534	3,685,162	4.5	77,883,372	95.5	77,298,568	94.8	584,804	0.7
WT CT22-2	52,553,912	2,188,434	4.2	50,365,478	95.8	49,973,839	95.1	391,639	0.7
KO CT02-1	87,958,970	5,035,981	5.7	82,922,989	94.3	82,154,491	93.4	768,498	0.9
KO CT02-2	72,625,320	4,309,937	5.9	68,315,383	94.1	67,951,245	93.6	364,138	0.5
KO CT06-1	97,903,638	4,891,173	5.0	93,012,465	95.0	92,226,211	94.2	786,254	0.8
KO CT06-2	52,322,684	3,458,587	6.6	48,864,097	93.4	48,471,980	92.6	392,117	0.7
KO CT10-1	93,163,248	5,070,280	5.4	88,092,968	94.6	87,043,158	93.4	1,049,810	1.1
KO CT10-2	67,001,700	2,491,212	3.7	64,510,488	96.3	63,975,834	95.5	534,654	0.8
KO CT14-1	53,923,978	2,591,525	4.8	51,332,453	95.2	50,914,274	94.4	418,179	0.8
KO CT14-2	62,996,908	3,710,214	5.9	59,286,694	94.1	58,591,773	93.0	694,921	1.1
KO CT18-1	78,528,680	3,837,671	4.9	74,691,009	95.1	74,073,533	94.3	617,476	0.8
KO CT18-2	43,988,742	2,981,222	6.8	41,007,520	93.2	40,621,094	92.3	386,426	0.9
KO CT22-1	52,579,070	2,238,152	4.3	50,340,918	95.7	49,913,641	94.9	427,277	0.8
KO CT22-2	80,434,378	3,190,342	4.0	77,244,036	96.0	76,594,491	95.2	649,545	0.8
average	68,007,013	3,329,458	4.9	64,677,556	95.1	64,111,669	94.2	565,887	0.8

Table 3　List of the rhythmic genes which are common in the four published papers (Koike et al., 2012; Menet et al., 2012; Vollmers et al., 2012; Yoshitane et al., 2014)

gene	CLOCK-ChIP-Seq at CT8
Nr1d1	1773.9
Dbp	1423.6
Mtss1	862.4
Per1	849.9
Klf13	826.1
Per2	807.5
Nr1d2	689.4
Tef	672.4
Fgfr2	555.9
Gys2	546.8
Usp2	502
Pcsk4	489.8
Gpr146	464.9
Thrsp	362
Hlf	329.4
Pik3ap1	312.2
Rorc	307.1
Wee1	276.7
Esrra	262
Cry1	261
Coq10b	250
Por	250
Efhd2	239.8
Nrg4	239
Upp2	239
St6gal1	223.9
Clmn	211.9
Ripk2	206
Ndrg1	199.9
Slc2a2	198
Nfil3	173.2
3010026O09Rik	167.3
Tenc1	167
Slc2a9	166.7
Arsa	166
Fkbp4	162
Ngef	161.2
Serpina6	157.8
Mknk2	149

gene	CLOCK-ChIP-Seq at CT8
Per3	140.4
Insig2	140
Rdh9	137.1
Litaf	132.3
Slc37a4	122.4
Klhdc7a	120.9
Cyp2a5	118.9
Marveld1	118
Odc1	117.5
Pnrc1	106.2
Ppfibp1	105
Stk35	102.9
Abhd6	98.8
St3gal5	98.8
Slc7a2	98.6
Steap3	98
Gpd1l	97
Elovl3	95.1
Eps8l2	95
Slc4a4	94
Arsg	90
Rnf125	89
Dtx4	88
Fpgs	85.9
Ddhd2	83
Stat5b	82.9
Abcg8	81
Adarb1	78.9
Rhbdd2	75
Cbs	73.2
Rcl1	72.5
Mthfr	70.9
Pde9a	68.6
Gldc	67.8
Homer2	66
Abca8b	65
Chka	65
Pnkd	63
Narf	61.8

gene	CLOCK-ChIP-Seq at CT8
Lrp4	61.5
Azin1	59.3
Abcg5	54
Ccrn4l	53
Acot3	50
Clock	48
Fmo5	47.3
Ivns1abp	47
Tars	46
Psen2	44
Syde2	43.3
Wdr6	42
Ptp4a1	41
Lrrc28	39
Gch1	37.4
Enpp1	36.9
Ppp1r3b	36.4
Lgals9	36
Fnip1	33.6
Fbxo21	32
Slc16a12	28.6
1300002K09Rik	24
Hal	21.7
Crip2	21.2
Ube2u	20
BC029214	17.7
Amt	17
Abcb11	0
Abtb2	0
Agpat6	0
Akr1c19	0
Appl1	0
Arntl	0
Atp1b1	0
Avpr1a	0
Casp6	0
Ccng2	0
Cldn1	0
Clec2h	0
Clpx	0
Cml5	0

gene	CLOCK-ChIP-Seq at CT8
Crot	0
D630039A03Rik	0
Ddc	0
Dhrs3	0
Enpp3	0
Fbxo6	0
Fkbp5	0
Fmo2	0
Gabarapl1	0
Gfod2	0
Grk5	0
Hacl1	0
Hsd3b5	0
Hsd3b7	0
Leo1	0
Mad2l2	0
Mreg	0
P2ry1	0
Pfkfb1	0
Ppard	0
Pxmp4	0
Rfxank	0
Slc16a5	0
Slc17a3	0
Slc30a10	0
Slc45a3	0
Slco1a4	0
Sort1	0
Spon2	0
St5	0
Syt1	0
Tob2	0
Trim24	0
Tsc22d3	0
Tsku	0
Tubb2a	0
Ypel2	0

Table 4　List of the rhythmic editing sites

chr	coordinate	editing region	gene_name	pvalue_WT	pvalue_KO
11	75300593	3'UTR	Rpa1	0.0001	0.0702
15	38491613	CDS	AZIN1	0.0002	0.3354
11	75300623	3'UTR	Rpa1	0.0004	0.0109
7	140135783	intergenic	intergenic	0.0005	0.09
19	44396424	3'UTR	Scd1	0.0008	0.0023
5	142669235	3'UTR	Wipi2	0.001	0.0354
2	18215357	3'UTR	Dnajc1	0.0012	0.1959
5	142669236	3'UTR	Wipi2	0.0016	0.0251
4	149118197	intronic	Dffa	0.0018	0.1521
7	140105799	3'UTR	Echs1	0.0022	0.5904
16	20123739	3'UTR	Klhl24	0.0024	0.166
7	140135784	intergenic	intergenic	0.0026	0.0369
3	58590823	3'UTR	2810407C02Rik	0.0034	0.0012
11	75176384	3'UTR	Ovca2	0.0037	0.613
2	132309633	3'UTR	Cds2	0.0038	0.0127
14	31700626	3'UTR	Ankrd28	0.0039	0.0122
7	79360769	3'UTR	Abhd2	0.0056	0.2405
19	4763089	intronic	uc008gap.1	0.006	0.368
X	56587643	3'UTR	Mmgt1	0.0065	0.0278
16	32299847	3'UTR	Rnf168	0.007	0.0626
10	128800572	3'UTR	Mmp19	0.0074	0.0368
5	142669249	3'UTR	Wipi2	0.0075	0.0194
10	128800569	3'UTR	Mmp19	0.0076	0.1509
11	77520357	3'UTR	Abhd15	0.0082	0.2463
16	32299854	3'UTR	Rnf168	0.0098	0.3519
1	133138010	3'UTR	Ppp1r15b	0.0112	0.0894
11	3150400	intronic	Sfi1	0.0114	0.0406
9	103086056	3'UTR	Slco2a1	0.0118	0.0441
10	76555590	intergenic	intergenic	0.0127	0.2813
X	56587644	3'UTR	Mmgt1	0.0147	0.0022
18	56956934	3'UTR	C330018D20Rik	0.0148	0.0593
8	40917790	3'UTR	Slc7a2	0.0149	0.1675
17	24176489	3'UTR	Tbc1d24	0.0149	0.3372
2	132309669	3'UTR	Cds2	0.0151	0.0199
14	32296625	3'UTR	Parg	0.0154	0.7145
3	87921521	intronic	Mrpl24	0.0162	N.D.
5	142669292	3'UTR	Wipi2	0.0174	0.163
11	75300618	3'UTR	Rpa1	0.0175	0.1357
14	31700662	3'UTR	Ankrd28	0.0195	0.4835
16	97857208	3'UTR	C2cd2	0.0205	0.0524
8	40917799	3'UTR	Slc7a2	0.021	0.0993
2	132309655	3'UTR	Cds2	0.0213	0.0034

5	87011887	3'UTR	Ugt2b35	0.0216		0.0168
15	9199472	intergenic	intergenic	0.0222		0.4463
14	72539504	3'UTR	Fndc3a	0.0225		0.0326
12	70995129	intergenic	intergenic	0.0228		0.3203
17	33928729	3'UTR	Tapbp	0.0231		0.3766
4	103164712	3'UTR	Mier1	0.0236		0.3073
14	52294229	3'UTR	Tox4	0.0239		0.052
8	124894122	3'UTR	Exoc8	0.0245		0.2811
18	56956940	3'UTR	C330018D20Rik	0.0253		0.1439
18	56956572	3'UTR	C330018D20Rik	0.0263		0.2708
4	45377142	3'UTR	Dcaf10	0.0267		0.0306
4	129309987	3'UTR	Rbbp4	0.0267		0.3447
11	75300610	3'UTR	Rpa1	0.0283		0.1184
14	21797711	3'UTR	Samd8	0.0283		0.0638
3	96632458	3'UTR	Rbm8a	0.0293		0.0983
10	128799433	3'UTR	Mmp19	0.0297		0.0265
10	76555582	intergenic	intergenic	0.0299	N.D.	
8	40920188	3'UTR	Slc7a2	0.0302		0.1134
15	55255640	3'UTR	uc007vsb.1	0.0304		0.231
17	35857734	3'UTR	Mdc1	0.0309		0.2627
14	75719719	CDS	Cog3	0.0316		0.368
2	118869941	intronic	Ivd	0.0319	N.D.	
11	75300578	3'UTR	Rpa1	0.0334		0.0691
9	96057240	intergenic	intergenic	0.0363		0.8563
8	72482670	3'UTR	Slc35e1	0.0364		0.0128
7	140136607	intergenic	intergenic	0.0392		0.1365
2	30203359	intronic	Ccbl1	0.0396	N.D.	
19	7538115	3'UTR	Atl3	0.0411		0.3527
11	75176432	3'UTR	Ovca2	0.0412		0.2448
8	72482340	3'UTR	Slc35e1	0.0416		0.0111
2	91015870	3'UTR	Celf1	0.0429		0.0793
3	96632460	3'UTR	Rbm8a	0.0439		0.096
2	126891517	3'UTR	2010106G01Rik	0.0442		0.2026
10	86836358	3'UTR	Nt5dc3	0.0453		0.0561
8	40920192	3'UTR	Slc7a2	0.0458		0.1369
5	135909342	3'UTR	Ywhag	0.0477		0.1311
12	100871715	3'UTR	9030617O03Rik	0.0483		0.0763
15	3280063	3'UTR	Sepp1	0.0483		0.4002
3	87921526	intronic	Mrpl24	0.0491		0.247
7	35391298	3'UTR	Rhpn2	0.0491		0.5125
15	55255254	3'UTR	uc007vsb.1	0.0493		0.0028
12	112958242	intergenic	intergenic	0.0497		0.3197
15	55255566	3'UTR	uc007vsb.1	0.0497		0.3052
6	72432367	intergenic	intergenic	0.0499		0.4689
15	81454965	intergenic	intergenic	0.0503		0.3546
15	38491612	CDS	AZIN1	0.0504		0.0063

11	75301040	3'UTR	Rpa1	0.0515		0.4453
14	31700663	3'UTR	Ankrd28	0.0523		0.0315
15	55255684	3'UTR	uc007vsb.1	0.0532		0.0424
11	35787911	3'UTR	Pank3	0.0542		0.1476
8	3539445	intronic	Pnpla6	0.0552		0.3922
15	55255642	3'UTR	uc007vsb.1	0.0554		0.1802
8	124894190	3'UTR	Exoc8	0.0557		0.4832
10	87931707	3'UTR	Igf1	0.0566		0.0019
14	8165933	intergenic	intergenic	0.0585		0.0712
11	75300631	3'UTR	Rpa1	0.0586		0.207
7	79360851	3'UTR	Abhd2	0.0587		0.0929
8	40920142	3'UTR	Slc7a2	0.0596		0.1756
2	118869942	intronic	Ivd	0.0597		0.3372
3	116744664	3'UTR	Agl	0.0607		0.3893
6	72432366	intergenic	intergenic	0.061		0.2033
2	163467539	intergenic	intergenic	0.0649		0.1349
X	150985455	3'UTR	Gnl3l	0.0652		0.0733
8	40917864	3'UTR	Slc7a2	0.0668		0.1153
10	86837257	3'UTR	Nt5dc3	0.0688		0.1759
7	140136552	intergenic	intergenic	0.0696		0.0229
14	7936048	CDS	Flnb	0.0728	N.D.	
2	5897957	intergenic	intergenic	0.073		0.2597
3	95183582	3'UTR	Gabpb2	0.0738		0.5212
8	124893874	3'UTR	Exoc8	0.076		0.2899
4	21911667	3'UTR	Coq3	0.078		0.2495
8	124893811	3'UTR	Exoc8	0.0782		0.551
6	91758167	3'UTR	Slc6a6	0.0782		0.4483
1	172092348	CDS	COPA	0.0784	N.D.	
5	113087834	3'UTR	2900026A02Rik	0.079		0.1087
7	39567651	intergenic	intergenic	0.0816		0.256
19	46595159	3'UTR	Sfxn2	0.0826		0.471
10	128800542	3'UTR	Mmp19	0.0827		0.0921
11	75177471	3'UTR	Ovca2	0.0827		0.4764
15	99728210	intergenic	intergenic	0.0843		0.5446
2	18214656	3'UTR	Dnajc1	0.0853		0.1293
7	140135775	intergenic	intergenic	0.086		0.0806
2	18215359	3'UTR	Dnajc1	0.0872		0.3744
8	40917777	3'UTR	Slc7a2	0.0882		0.5642
X	150985497	3'UTR	Gnl3l	0.0892		0.2143
14	31700629	3'UTR	Ankrd28	0.0909		0.0605
17	35474554	3'UTR	H2-Q10	0.0916		0.2712
4	155621904	3'UTR	Slc35e2	0.0944		0.1805
17	46774937	3'UTR	Rpl7l1	0.0988		0.2286
19	46595175	3'UTR	Sfxn2	0.0995		0.0058